

N7776447



Georgia Institute of Technology
School of Mechanical Engineering
Atlanta, Georgia

PREDICTION OF CRYOGENIC HEAT PIPE PERFORMANCE

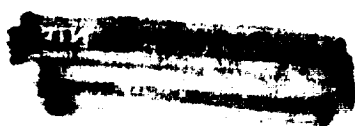
Final Report

Prepared for the
National Aeronautics and Space Administration
under
Grant NSG-2054

Prepared by
Gene T. Colwell, Professor

March 31, 1977

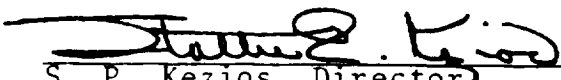





Georgia Institute of Technology
School of Mechanical Engineering
Atlanta, Georgia
30332

NASA Grant NSG-2054
Final Report
March 31, 1977

Approved:


S. P. Kezios, Director
School of Mechanical Engineering


Gene T. Colwell
Principal Investigator

ACKNOWLEDGEMENTS

The author wishes to express his gratitude to Stan Ollendorf of the Goddard Space Flight Center for continued encouragement and advice over the past two years. In addition Al Sherman of the Goddard Space Flight Center and Craig McCreight of the Ames Research Center contributed greatly to the project.

SUMMARY

This report describes work performed in the School of Mechanical Engineering at the Georgia Institute of Technology under NASA grant NSG-2054. The project was started in January of 1975 and completed in March of 1977. Two M.S. theses [8,28], which are directly related to the project, have been published and it is expected that at least one paper will be published in a technical journal as a result of work performed under the grant.

The main goal of the work has been to study theoretically the transient behavior of very low temperature heat pipes. A powerful technique has been developed for predicting transient three dimensional temperature distributions and heat fluxes for heat pipes operating under a wide variety of conditions. Radiating, conducting, and convecting external environments can be handled. In addition, startup from the supercritical state can be accommodated.

TABLE OF CONTENTS

	Page
ACKNOWLEDGEMENTS.	i
SUMMARY	ii
LIST OF TABLES.	v
LIST OF ILLUSTRATIONS	vi
NOMENCLATURE.	viii
I. INTRODUCTION.	I
A. Statement of Problem	
B. Background	
C. Literature Survey	
II. THEORETICAL DEVELOPMENT	8
A. Description of Digital Model	
B. Solution Methods	
C. Fluid Dynamic Effects	
D. Logic Solution	
E. Description of Analog Model	
III. RESULTS AND COMPARISONS	37
IV. CONCLUSIONS AND RECOMMENDATIONS	58
APPENDICES	
A. TRANSFORMATION OF COORDINATE SYSTEMS.	61
B. THERMODYNAMIC PROPERTY.	64
C. WICK-WALL INTERFACE NODES	66
D. COMPUTER CODE	69
E. DISCUSSION OF STABILITY AND ACCURACY OF NUMERICAL TECHNIQUES.	86

	Page
F. CALCULATION OF THERMAL CONDUCTIVITY.	88
G. ANALOG SCALING	90
H. DERIVATION OF EXPONENTIAL MODEL.	92
REFERENCES	93
DISTRIBUTION	96

LIST OF ILLUSTRATIONS

Figure	Page
1. General Layout of Heat Pipe.	10
2. Closeup of Composite Slab and Circumferential Wick at Heat Transfer Section.	11
3. Capillary Structure.	12
4. Heat Pipe Model.	13
5. Computation Grid and Boundary Conditions	21
6. Cooling Jacket Used in Model	24
7. Model of Fluid Flow in Slab.	25
8. Flow Diagram of Computer Program	29
9. Schematic Diagram of Analog Model.	34
10. Analog Circuit	35
11. Comparison of Model with Experimental Data from the Literature.	38
12. Comparison of Exponential, Analog and Digital Models for Heat Pipe with Cooling Jacket	40
13. Comparison of Analog and Digital Model for Case 1	42
14. Effect of Changing Wall Thickness.	44
15. Effect of Changing Number of Wick Layers	45
16. Effect of Changing Thickness of Fluid Gap.	46
17. Effect of Changing Slab Compositions	47
18. Comparison of Startup at Different Power Levels.	48
19. Comparison of Startup at Different Temperatures.	50

Figure	Page
20. Development of Overall Temperature Gradients. . .	51
21. Comparison of Heat Pipe Response with Cooling Jacket or Radiating Surface Heat Sink	52
22. Response of Radiating Heat Sink	53
23. Startup from Supercritical.	54
24. Comparison of Predicted Fluid Velocity with Data from Literature.	55
25. Velocity with Position in Composite Slab.	57
26. Polar to Rectangular Transformation	63
27. Wick-Wall Interface Nodes	67

NOMENCLATURE

A_C	cross-sectional area of slab
A_i	constant coefficient for node i
A_R	surface area of radiator
B_i	constant coefficient for node i
c_{CJ}	composite specific heat for cooling jacket
c_f	specific heat of coolant
C_i	constant coefficient for node i
c_p	specific heat of pipe wall
c_R	specific heat of radiator
c_T	composite specific heat for total system
c_V	composite specific heat for vapor region
c_w	composite specific heat for screen and fluid gaps
d_f	distance between filament centers in screen
D_i	constant coefficient for node i
h_C	surface coefficient
h_{fg}	heat of vaporization of working fluid
\bar{K}	effective inverse permeability of slab
K_p	thermal conductivity of pipe wall
K_w	thermal conductivity of wick
L	distance from fluid source to fluid front in slab
ℓ_C	condenser length
ℓ_E	evaporator length
\dot{m}	mass flow rate of working fluid in slab

m_{CJ}	mass of cooling jacket and fluid
\dot{m}_f	mass flow rate of coolant
m_R	mass of radiating heat sink
m_T	total mass of heat pipe and cooling jacket
m_V	total mass of vapor region
NIC	number of radial nodes in condenser grid
NIE	number of radial nodes in evaporator grid
NJE	number of circumferential nodes in evaporator grid
NKC	number of axial nodes in condenser grid
NKA	number of axial condenser nodes in adiabatic section
NL	number of layers of screen in wick
Q_{cap}	capillary limited heat transfer rate
Q_E	Heat flux at evaporator surface
Q_{max}	maximum heat transfer rate for scaling analog
Q_{space}	heat flux into radiator from space
r	radial coordinate
r_B	inner radius of pipe wall
r_f	filament radius in screen
r_I	inner radius of wick
r_i	radius at node i
r_O	outer radius of pipe wall
r_p	pore radius of screen
SF	scaling factor for wick nodes
$T_{1,2,\dots,6}$	temperature of node 1, 2, ..., 6 in analog model
t	time
t_{max}	representative time used for scaling analog

T_{CJ}	temperature of cooling jacket
T_C	temperature of condenser
$TC_{i,k}^n$	temperature of condenser node i,k at time n
T_E	temperature of evaporator
$TE_{i,j}^n$	temperature of evaporator node i,j at time n
T_I	incoming temperature of coolant
T_{min}	minimum temperature for scaling analog
T_{max}	maximum temperature for scaling analog
T_R	temperature of radiator
T_V	temperature of vapor region
V	velocity of fluid in slab
v_{pC}	volume of pipe wall in condenser
v_{pE}	volume of pipe wall in evaporator
v_{wC}	volume of wick in condenser
v_{wE}	volume of wick in evaporator
x	transformed radial coordinate
y	transformed circumferential coordinate
z	axial coordinate
α	thermal diffusivity
β	width of fluid gap
Δ	finite difference operator
ϵ	emmisivity of radiator
μ_ℓ	viscosity of liquid nitrogen
ρ_ℓ	density of liquid nitrogen
ρ_p	density of pipe wall
ρ_w	density of wick

σ	Stefan-Boltzman constant
σ_l	surface tension of liquid nitrogen
ϕ	circumferential coordinate in evaporator

xii, xiii, xiv

LIST OF TABLES

Table		Page
1.	Dimensions and Materials of Heat Pipe Considered in this Study.	9
2.	Parameters for Case Studies	41

I. INTRODUCTION

A. Statement of Problem

Investigations into the performance of cryogenic heat pipes have been in progress at the Georgia Institute of Technology for several years. In continuation of these investigations the goal of this study has been to gain a better understanding of the transient response of cryogenic heat pipes and heat pipe systems. A method for predicting behavior of heat pipes during startup or changes in thermal transport has been developed. Included in the model are provisions for simulating startup from temperatures above the critical point of the working fluid.

B. Background

A heat pipe is a device that transfers large quantities of heat with a relatively small temperature gradient. The containing envelope has an internal wick structure and a liquid in near equilibrium with its vapor phase. The phenomena of conduction and phase change are combined to make high thermal conductance possible. The basic theory, design, and operation of heat pipes are well discussed by Cotter [1], Chisolm [2], and others.

As heat is added to the evaporator of a heat pipe

some of the fluid in the wick evaporates thus increasing the vapor pressure. The increased pressure drives some of the warm vapor to the condenser. The condensing vapor gives up energy which is conducted through the wall and transferred from the heat pipe. Due to evaporation the liquid-vapor interface recedes into the capillary structure and thus decreases the radius of curvature of the meniscus in the heated end. Condensation on the capillary structure at the cool end increases the meniscus radius in the condenser. This difference in radii of curvature creates the driving force to pump the liquid back to the evaporator [1].

The heat pipe startup mode described above assumes the vapor density at the ambient temperature is high enough for a continuum flow to exist and that the capillary structure is filled with working fluid. Such startup is referred to as uniform startup by Cotter [3]. A second mode of startup occurs if the vapor pressure is low and molecular flow exists at ambient temperatures. Heating produces a continuum in the evaporator and transition zone between the evaporator and condenser. Often the working fluid is in a frozen state and must melt before startup can occur. This mode takes about two and one half times longer than uniform startup assuming the working fluid is not frozen prior to startup. Non-condensable gases, when present in the vapor space, creates a third mode of startup. During heating the non-condensables are swept into the cold end of the condenser.

This method of startup can be accomplished very quickly or very slowly depending on the quantity of non-condensables present.

At steady state, for some types of capillary structures, that part of the evaporator capillary furthest from the condenser may be dried out. The wick geometry and meniscus radius determine how much of the evaporator is actively working. Colwell and Williams [4] suggested that the axial vapor Reynolds number may determine the length along which condensation actually occurs in the condenser. Assuming a saturated wick before startup the development of these phenomena do affect startup times.

If the heat pipe is at a temperature above the critical point of the working fluid before startup, all of the fluid will be in a single phase supercritical state. Before the evaporation-condensation cycle can begin the fluid must first be cooled below the critical temperature at the cool end. Capillary action will then pump the liquid along the wick back to the evaporator. The velocity of the fluid in the wick is on the order of centimeters per minute [5]. The entire heat pipe must be reflexed before any significant heat transfer can take place.

In the design of a heat pipe system it is important to understand the startup of the system and the response to a change in power level. The parameters affecting transient response of a heat pipe must be determined. The goal of

this project was to develop a technique for predicting the startup and response times for various heat pipes.

C. Literature Survey

The performance of heat pipes in an outer space environment was evaluated by Kirkpatrick and Brennan [6] using the Applications Technology Satellite (ATS-F). They concluded that for space applications heat pipes can be useful temperature control devices. Sherman and Brennan [7] performed a study of low temperature heat pipes for spacecraft uses. Nitrogen and oxygen were determined to be best fluids for operation in the cryogenic temperature range. The composite slab wick was said to be a reliable porous media for present day and projected NASA applications.

Recent work at the Georgia Institute of Technology has been directed to understanding the steady state performance of a heat pipe similar to the one in this study. Hare [8] performed a theoretical study of a performance of a cryogenic heat pipe using nitrogen as the working fluid. Polynomial expressions were developed for predicting the thermal properties as a function of temperature. Mass- and heat-transport equations were combined to give capillary and sonic limitations on the performance of the pipe and the thermal resistances of each heat pipe component. A study was made on the effects of changing the composite slab and wick structure.

Colwell [9] used a similar approach to study the effects

of fluid gaps in the circumferential wick. Partial dryout and vapor Reynolds number effect were added through a simplified approach. The effect of changing wall thickness, number of wick layers and mesh size was also modeled.

A coupled heat transfer diffusion model was used by Saaski [26] to model a gas controlled heat pipe. The device was 45.48 cm long with an inside radius of 1.288 cm and used methanol as the working fluid. Experimental response curves were compared with curves predicted with the model. Agreement is very good, both curves reaching 95 percent of steady state values in about 130 seconds.

In a study of the dynamic behavior of heat pipes Groll, et al. [10] determined that small power variations around the operating point of a heat pipe present no special problems. The discussion is primarily concerned with heat pipes in the 200 K to 500 K temperature range. A one-dimensional model was developed for prediction of heat pipe response and examples of normal startup and startup failure were presented. Groll concluded that the dynamic response of heat pipes can be adequately treated with a simple mathematical model.

Another startup model was developed by Cotter [3]. Linear relationships were found for predicting uniform startup and startup with non-condensable gases present. Various modes of heat pipe startup are described and mechanisms which might affect successful startup are discussed. From this model the response time for most high performance heat pipes

is between 10 and 100 seconds.

Chato and Streckert [5] ran a series of tests with a water heat pipe. The device was 81.9 cm long with an inside diameter of 7.62 cm. Experimental values of maximum heat flux were in the middle of the range predicted by horizontal wicking tests. During normal operation, temperatures in the vapor region did not vary by more than $1/2^{\circ}\text{C}$. Attempts to measure transients failed since the heat pipe responded faster than the heating and cooling system. They estimated the response time of the heat pipe at less than twenty seconds.

Smirnov, et al. [11] developed a model for predicting startup of gas controlled heat pipes. Their calculations were in good agreement with experimental results. The dynamic response of buffered and unbuffered heat pipes was modeled by Rice and Azad [12]. Their model agreed with experimental data for a sodium heat pipe and for a water heat pipe.

To operate, a heat pipe must have a source and sink. Any measured response must take the source and sink into account. Should the heat sink radiate the incoming energy a phenomenon referred to by Anand, et al. [13] as temperature choking takes place. The radiating surface must adjust its temperature up or down to be in equilibrium with the incoming energy. This movement in turn forces the heat pipe to adjust its operating temperature. The response of such a system would be different from a system with a condenser bath for cooling.

Calimbas and Hulett [14] ran tests on an avionic heat pipe. The device used water as a working fluid. The inside diameter was 6.35 cm and it was 60.96 cm long. Condenser cooling was accomplished by a forced air heat exchanger. The system took fifteen minutes to adjust to a change in the heater level.

A water heat pipe with a glass bead capillary structure was built and tested by Cosgrove, et al. [15]. Cooling was accomplished by evaporation of methanol. A steady state model was developed consisting of basic mass, energy and momentum balances. Predicted values were in close agreement with experimental results. After a change in power approximately thirty-five minutes were required for the system to reach a steady state.

All of the literature indicates that heat pipes have very small response times. Since the mass of heating and cooling systems is greater than that of a heat pipe they respond more slowly. Transient data from experiments reflect the response time of the heaters and cooling jackets used in the experiments. Any attempt to model such a system must include an accurate model of the heating and cooling apparatus.

II. THEORETICAL DEVELOPMENT

This study is concerned with a cryogenic heat pipe with a composite slab wick. Geometry and physical characteristics were suggested by the sponsoring agency. Dimensions and materials are given in Table 1 and Figure 1. The configuration of the composite slab and wick is shown in Figures 2 and 3.

The response of this heat pipe has been studied on analog and digital computers. A system of nodes is used to develop a set of time dependent equations accounting for the heat capacity of the system. Due to a limited capacity, the nodal system used for the analog model is fairly simple and limited to small transient. The model assumes constant properties and does not include any effects of fluid dynamics. The digital model includes a much finer nodal system and fluid dynamics. Property equations in the program permit the variation of properties with temperature. Both models predict response and temperature profiles for the heat pipe.

A. Description of the Digital Model

For the digital model the heat pipe is broken into its three main parts: evaporator, vapor region, and condenser which includes the adiabatic section. Figure 4 shows the

Table 1. Dimensions and Materials for the Heat Pipe
Considered in this Study

Total length	.9144 meters
Length of evaporator	.1524 meters
Length of condenser	.3048 meters
Length of adiabatic section	.4572 meters
Outside diameter of pipe	.635 centimeters
Wall thickness	.1015 centimeters
Working fluid	Nitrogen
Material of pipe and capillary structure	304 stainless steel
Wick configuration	circumferential wick with composite central slab
Slab	4 layers 400 mesh around 5 layers 30 mesh screen
Circumferential wick	2 layers 400 mesh screen
Fluid gap	.003048 centimeters

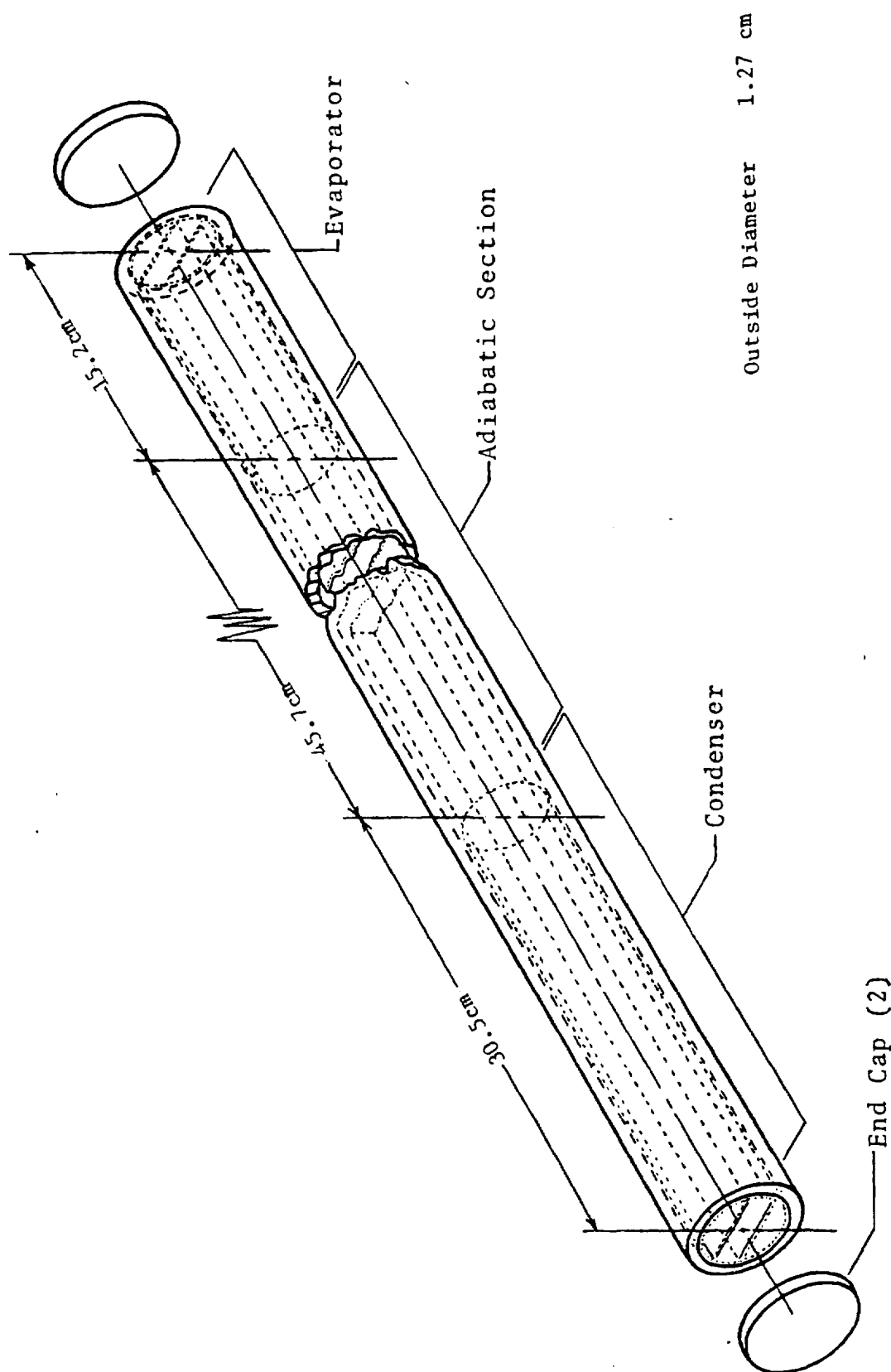


Figure 1. General Layout of Heat Pipe

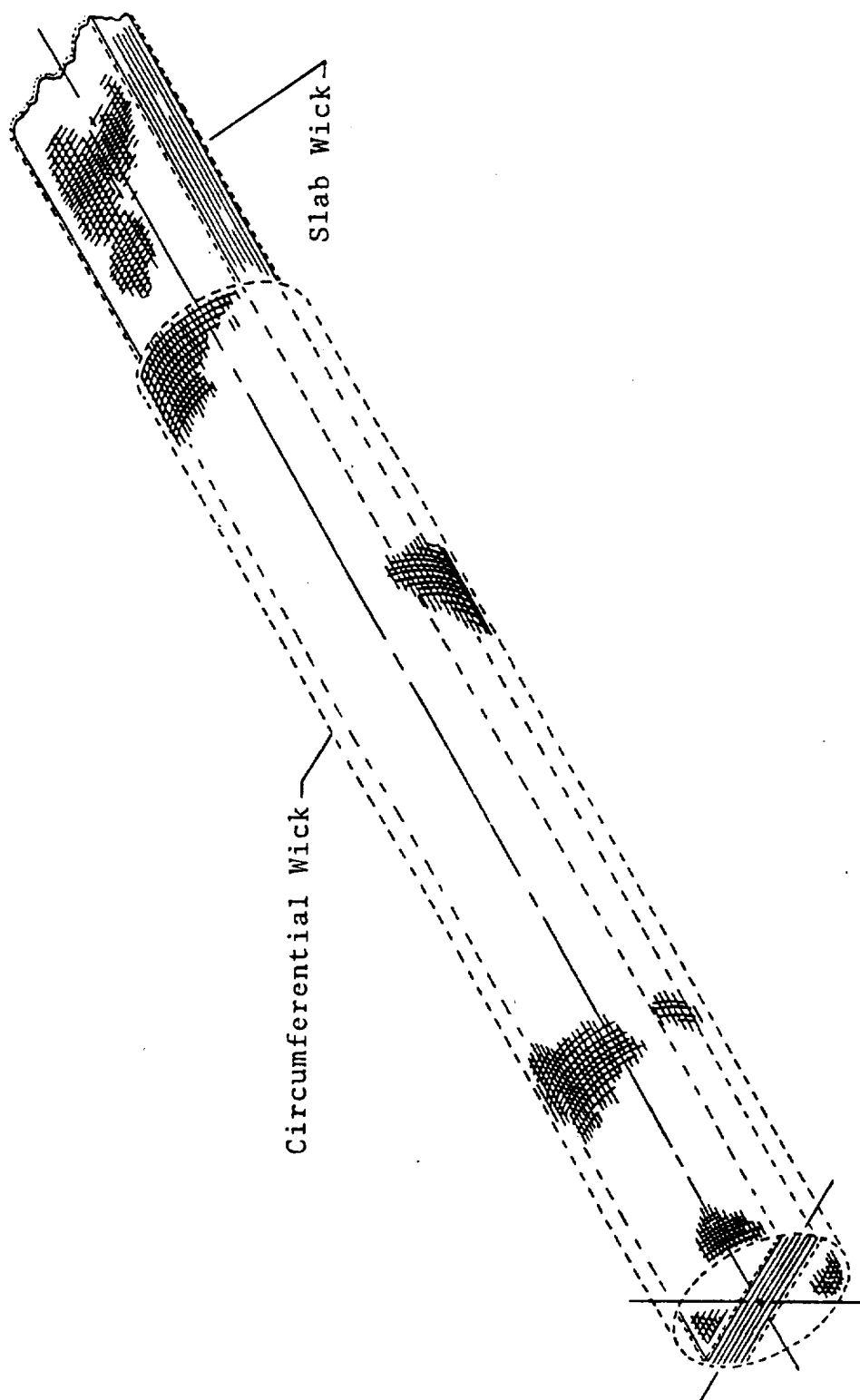


Figure 2. Close-Up of Composite Slab and Circumferential Wick
at Heat Transfer Section

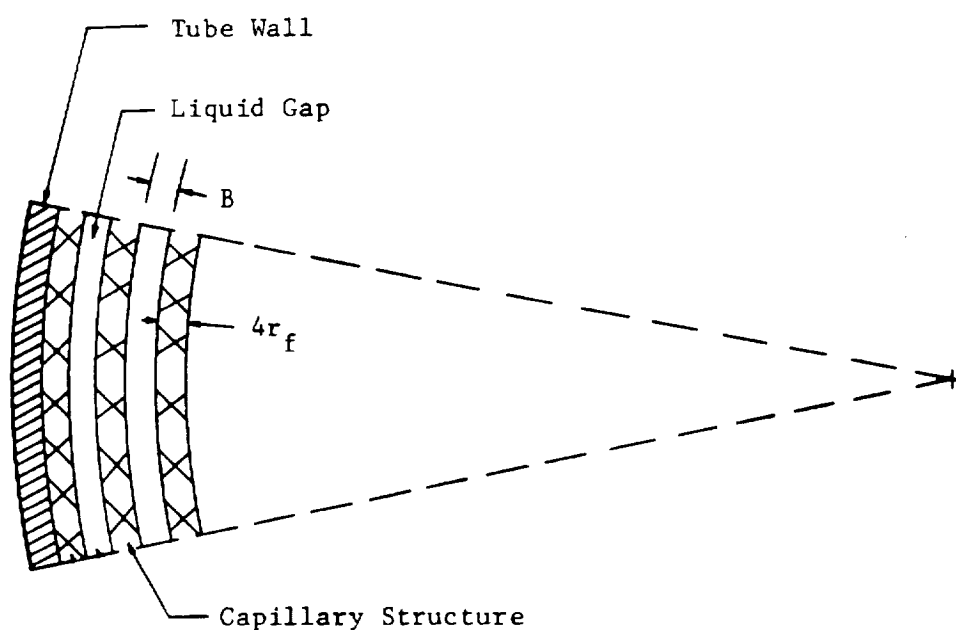


Figure 3. Capillary Structure

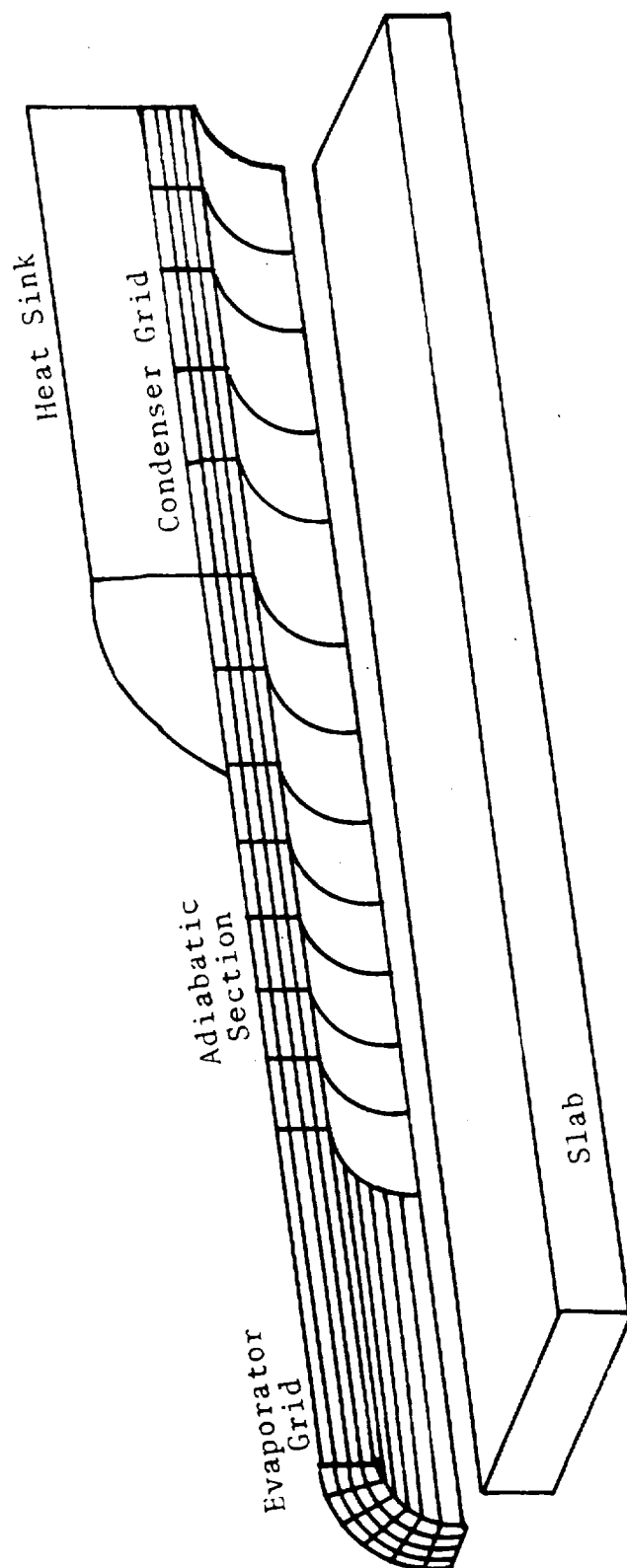


Figure 4. Heat Pipe Model

parts of the heat pipe and the nodal system used for solutions. Basic heat transfer equations are written for each part and the equations are coupled at the boundaries.

A two-dimensional model of the evaporator has been developed that permits temperature variation in the radial and circumferential directions. Symmetry is assumed such that only a 90° section is modeled. In this way the effects of partial burn-out in the circumferential wick can be studied.

The vapor region is modeled as a lumped mass system. The system includes the vapor, the slab, and the innermost part of the wick along the entire length of the heat pipe. The vapor temperature is assumed to vary only with time having the same value in both the evaporator and condenser.

Condenser and adiabatic sections are modeled as two dimensional in the radial and axial directions. This arrangement permits study of Reynolds number effects and axial conduction.

Conditions at the surface of the evaporator and condenser can be modeled in several ways. The surface temperature can be fixed, a known heat flux can be made to exist at the surface, or an evaporator or condenser saddle can be added. The condenser saddle can be cooled with a cooling jacket or a radiating surface.

B. Solution Methods

Basic heat transfer equations can be written for each

section of the heat pipe. The result is a system of three coupled differential equations:

Evaporator:

$$\frac{1}{\alpha} \frac{\partial T_E}{\partial t} = \frac{\partial^2 T_E}{\partial r^2} + \frac{1}{r} \frac{\partial T_E}{\partial r} + \frac{1}{r} \frac{\partial^2 T_E}{\partial \phi^2} + \frac{\partial^2 T_E}{\partial z^2} \quad (2.1)$$

Vapor:

$$m_V c_V \frac{dT_V}{dt} = 2\pi r_I \ell_E K_W \left. \frac{\partial T_E}{\partial r} \right|_{r=r_I} + 2\pi r_I \ell_C K_W \left. \frac{\partial T_C}{\partial r} \right|_{r=r_I} \quad (2.2)$$

Condenser:

$$\frac{1}{\alpha} \frac{\partial T_C}{\partial t} = \frac{\partial^2 T_C}{\partial r^2} + \frac{1}{r} \frac{\partial T_C}{\partial r} + \frac{\partial^2 T_C}{\partial z^2} \quad (2.3)$$

These equations are transient conduction equations and do not account for fluid dynamics directly. As will be shown in the next section, in uniform startup with a fully wetted wick the time for fluid velocity response is very small. In the case of startup from the supercritical, these effects can be handled by manipulation of boundary conditions in the nodal system.

The equation for the vapor region is first order in time only. Finite difference techniques permit solving for the vapor temperature explicitly at each time step. The

equation can be written in finite difference form as:

$$m_V c_V \frac{T_V^{n+1} - T_V^n}{t^{n+1} - t^n} = \frac{2\pi r_I \ell_E K_W}{NJE \Delta x r_I} \sum_{j=1}^{NJE} (TE_{NIE-1,j}^n - T_V^n) + \frac{2\pi c_I \ell_C K_W}{NKC \Delta x c_I} \sum_{k=1}^{NKC} (TC_{NIC-1,k}^n - T_V^n) \quad (2.4)$$

Which can be solved explicitly

$$T_V^{n+1} = \frac{2\pi \ell_E K_W \Delta t}{NJE \Delta x m_V c_V} \sum_{j=1}^{NJE} (TE_{NIE-1,j}^n - T_V^n) + \frac{2\pi \ell_C K_W \Delta t}{NKC \Delta x m_V c_V} \sum_{k=1}^{NKC} (TC_{NIC-1,k}^n - T_V^n) + T_V^n \quad (2.5)$$

Note that the heat transfer into the vapor region is equated to the heat transfer across the inner nodes of the evaporator and condenser sections.

The partial differential equations that describe heat transfer in the evaporator and condenser sections can be solved with a grid system of nodes. The curvilinear system is made rectangular with a change of variables. Details of this variable change are given in Appendix A. A heat balance is written for each node equating net heat gain with the change in temperature of that node. The resulting systems of equations are solved with an alternating direction implicit method.

Two finite difference approximations of equation (2.1) are used alternately to sweep through the evaporator grid for each time step. These two equations are given by: For the first half time step

$$\begin{aligned} \rho_p c_p r_i^2 \frac{TE_{i,j}^{n+1/2} - TE_{i,j}^n}{t^{n+1/2} - t^n} = & \frac{K_p}{\Delta x^2} (TE_{i+1,j}^{n+1/2} + TE_{i-1,j}^{n+1/2} - 2TE_{i,j}^{n+1/2}) \\ & + \frac{K_p}{\Delta y^2} (TE_{i,j+1}^n + TE_{i,j-1}^n - 2TE_{i,j}^n) \\ & - \frac{K_p TE_{i,j}^n}{NJE \sum_{j=1} TE_{i,j}^n} \left(\sum_{j=1} NJE TE_{i,j}^n - TC_{i,1}^n \right) \left(\frac{r_i^2}{\Delta z^2} \right) \end{aligned} \quad (2.6)$$

And for the second half time step

$$\begin{aligned} \rho_p c_p r_i^2 \frac{TE_{i,j}^{n+1} - TE_{i,j}^{n+1/2}}{t^{n+1} - t^{n+1/2}} = & \frac{K_p}{\Delta x^2} (TE_{i+1,j}^{n+1/2} + TE_{i-1,j}^{n+1/2} - 2TE_{i,j}^{n+1/2}) \\ & + \frac{K_p}{\Delta y^2} (TE_{i,j+1}^{n+1} + TE_{i,j-1}^{n+1} - 2TE_{i,j}^{n+1}) \\ & - \frac{K_p TE_{i,j}^n}{NJE \sum_{j=1} TE_{i,j}^n} \left(\sum_{j=1} NJE TE_{i,j}^n - TC_{i,1}^n \right) \left(\frac{r_i^2}{\Delta z^2} \right) \end{aligned} \quad (2.7)$$

Note that the equations are implicit in only one direction and this direction changes with each half time step.

The last term in each equation accounts for heat conducted axially along the tube. An artificial node is created at the evaporator end of the adiabatic section. At each radial location the artificial node has a temperature equal to the average temperature of the evaporator nodes at that same radial location. This node provides a constant temperature boundary condition for the condenser and adiabatic grid. A weighted fraction of the total heat conducted axially is subtracted from each evaporator node.

Casting equation (2.6) in a different form gives

$$\begin{aligned}
 & - \left(\frac{\Delta t K_p}{2(\Delta x)^2 \rho_p c_p r_i} \right) TE_{i+1,j}^{n+1/2} + \left(1 + \frac{\Delta t K_p}{(\Delta x)^2 \rho_p c_p r_i} \right) TE_{i,j}^{n+1/2} \\
 & - \left(\frac{\Delta t K_p}{2(\Delta x)^2 \rho_p c_p r_i} \right) TE_{i-1,j}^{n+1/2} = \left(\frac{\Delta t K_p}{2(\Delta y)^2 \rho_p c_p r_i} \right) (TE_{i,j+1}^n + TE_{i,j-1}^n) \\
 & \quad \left(1 - \frac{\Delta t K_p}{(\Delta y)^2 \rho_p c_p r_i} \right) TE_{i,j}^n \\
 & - \left(\frac{\Delta t K_p}{2\rho_p c_p (\Delta z)^2} \right) \left(\frac{TE_{i,j}^n}{\sum_{j=1}^{NJE} TE_{i,j}^n} \right) \left(\frac{1}{NJE} \sum_{j=1}^{NJE} TE_{i,j}^n - TC_{i,1} \right) \quad (2.8)
 \end{aligned}$$

This equation can be used to construct a matrix of NIE equations for each value of j . Each equation is of the form:

$$A_i TE_{i-1,j}^{n+1/2} + B_i TE_{i,j}^{n+1/2} + C_i TE_{i+1,j}^{n+1/2} = D_i \quad (2.9)$$

and the resulting matrix is shown below:

$$\begin{vmatrix} B_1 & C_1 & 0 & \dots & \dots & 0 & 0 \\ A_2 & B_2 & C_2 & 0 & \dots & 0 & 0 \\ 0 & A_3 & B_3 & C_3 & \dots & 0 & 0 \\ \vdots & \vdots & \vdots & \vdots & \vdots & \vdots & \vdots \\ 0 & 0 & 0 & \dots & A_{NIE-1} & B_{NIE-1} & C_{NIE-1} \\ 0 & 0 & 0 & \dots & 0 & A_{NIE} & B_{NIE} \end{vmatrix} = \begin{vmatrix} D_1 \\ D_2 \\ \vdots \\ \vdots \\ D_{NIE} \end{vmatrix}$$

This matrix is tridiagonal and can be solved with a modified Gaussian elimination technique [16]. This particular subroutine permits any combination of boundary conditions at either end of the array. A matrix is constructed and solved for each value of j giving values at each location for the first half time step. The second equation (2.7) is then used to construct and solve a matrix of NJE equations for each value of i . This solution technique is known as the alternating direction implicit. It has the advantage of being very stable with respect to time and yet being fairly simple to solve numerically.

A similar derivation in the condenser and adiabatic section gives:

$$\begin{aligned}
& - \left(\frac{\Delta t K_p}{2(\Delta x)^2 \rho_p c_p r_i} \right) TC_{i+1,k}^{n+1/2} + \left(1 + \frac{\Delta t K_p}{(\Delta x)^2 \rho_p c_p r_i} \right) TC_{i,k}^{n+1/2} \\
& - \left(\frac{\Delta t K_p}{2(\Delta x)^2 \rho_p c_p r_i} \right) TC_{i-1,k}^{n+1/2} = \left(\frac{\Delta t K_p}{2(\Delta z)^2 \rho_p c_p} \right) (TC_{i,k+1}^n + TC_{i,k-1}^n) \\
& + \left(1 - \frac{\Delta t K_p}{(\Delta z)^2 \rho_p c_p} \right) TC_{i,k}^n \tag{2.10}
\end{aligned}$$

In the formulation of the equations the thermal properties are assumed constant. Expressions were developed by Hare [8] which permitted evaluation of properties as a function of temperature. These expressions have been modified to work with International units and additional expressions have been developed for specific heats. Appendix B lists the polynomials used. These expressions are used to calculate new properties whenever the vapor temperature has changed by more than a specified amount.

Special coefficients are required for the interface of the pipe wall and the wick. These expressions are developed in Appendix C.

The three equations were coupled at the boundaries. Figure 5 is a schematic diagram of the computational grid and boundary conditions. The temperature of the innermost node of both evaporator and condenser is calculated as a part of the vapor region and held as a constant temperature

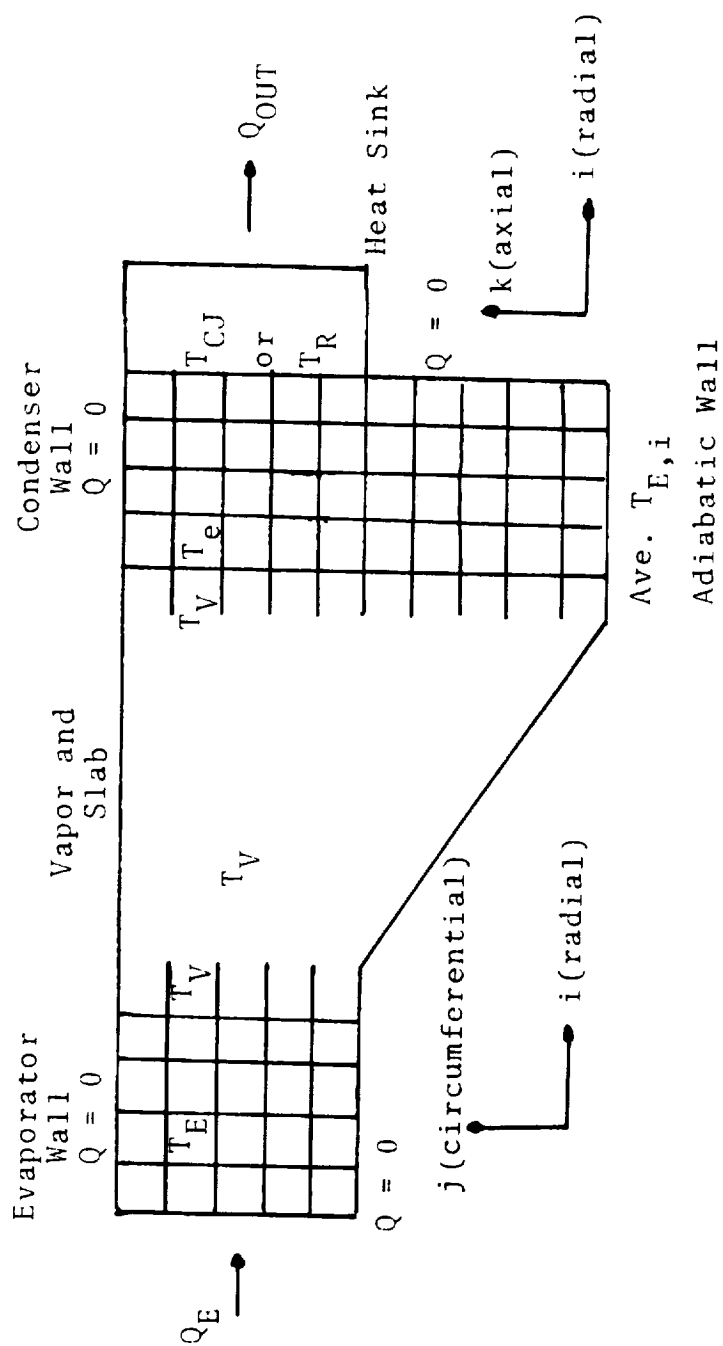


Figure 5. Computation Grid

boundary for both regions. Due to symmetry both ends of the evaporator grid can be assumed adiabatic. Also the outer surface of the adiabatic section and the lower end of the condenser are insulated. The vapor equation is in time only and therefore requires only an initial condition. Boundary conditions at the outer surface of the evaporator and condenser can be modified to better model the total system of which the heat pipe is a part.

Cooling of the condenser saddle can be accomplished either of two ways. For a radiating condenser a heat balance gives

$$m_R c_R \frac{dT_R}{dt} = 2\pi r_O l_C h_C (T_C - T_R) - A_R \sigma \epsilon T_R^4 + Q_{space}$$

which can be solved explicitly as:

$$T_R^{n+1} = \frac{2\Delta t \rho r_O \Delta z h_C}{m_R c_R} \sum_{k=NKA+1}^{NKC} (T_{NIC,k}^n - T_R^n) - \frac{A_R \sigma \epsilon \Delta t}{m_R c_R} T_R^{n4} + \frac{Q_{space}^n \Delta t}{m_R c_R} + T_R^n$$

If a cooling jacket is to be used the following equation has to be solved:

$$m_{CJ} c_{CJ} \frac{dT_{CJ}}{dt} = 2\pi r_O l_C h_C (T_C - T_{CJ}) + \dot{m}_f c_f (T_I - T_{CJ})$$

or

$$T_{CJ}^{n+1} = \frac{2\Delta t \pi r_0 \Delta z h_C}{m_{CJ} c_{CJ}} \sum_{k=NKA+1}^{NKC} (T_{NIC,k}^n - T_{CJ}^n) + \frac{\dot{m}_f c_f \Delta t}{m_{CJ} c_{CJ}} (T_I^n - T_{CJ}^n) + T_{CJ}^n$$

This equation assumes a cooling jacket as shown in Figure 6. Both of these heat sink models are coupled to the condenser with a surface coefficient.

C. Fluid Dynamic Effects

If the startup of a heat pipe is to proceed smoothly fluid must be able to reach the evaporator capillary structure at the same rate that evaporation occurs. Fluid flow in the slab can be modeled as shown in Figure 7. A one dimensional momentum balance can be written for the case where evaporator burnout has occurred:

$$\frac{2\sigma_\ell}{r_p} A_c - \bar{K} \frac{\mu_\ell \dot{m} L}{\rho_\ell A_c} A_c = \frac{d}{dt} (A_c L V_{\rho\ell}) \quad (3.1)$$

If the length is assumed equal to the distance from the midpoint of the condenser to the midpoint of the evaporator the equation can be solved for the velocity as a function of time. The result is:

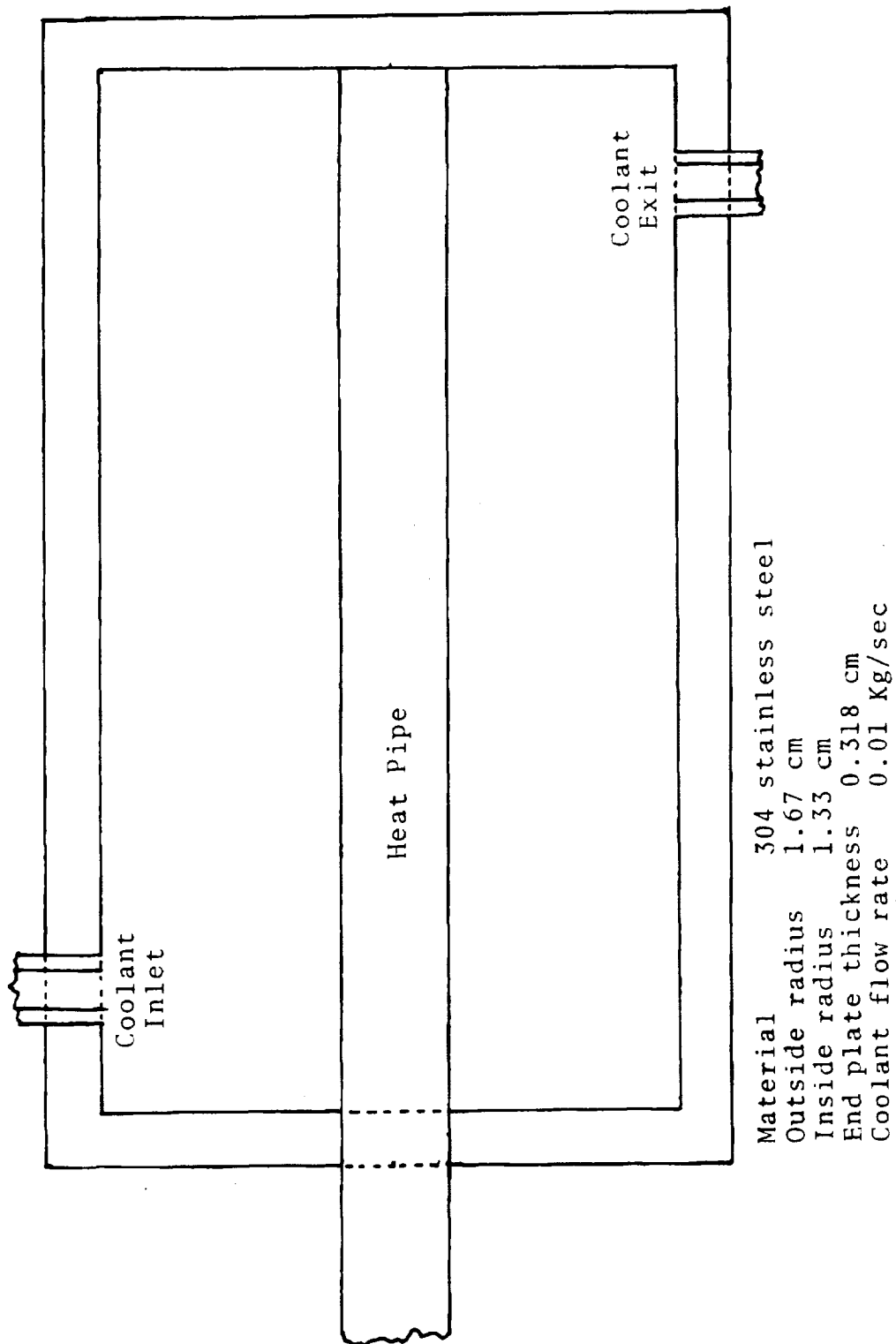


Figure 6. Cooling Jacket Used in Model

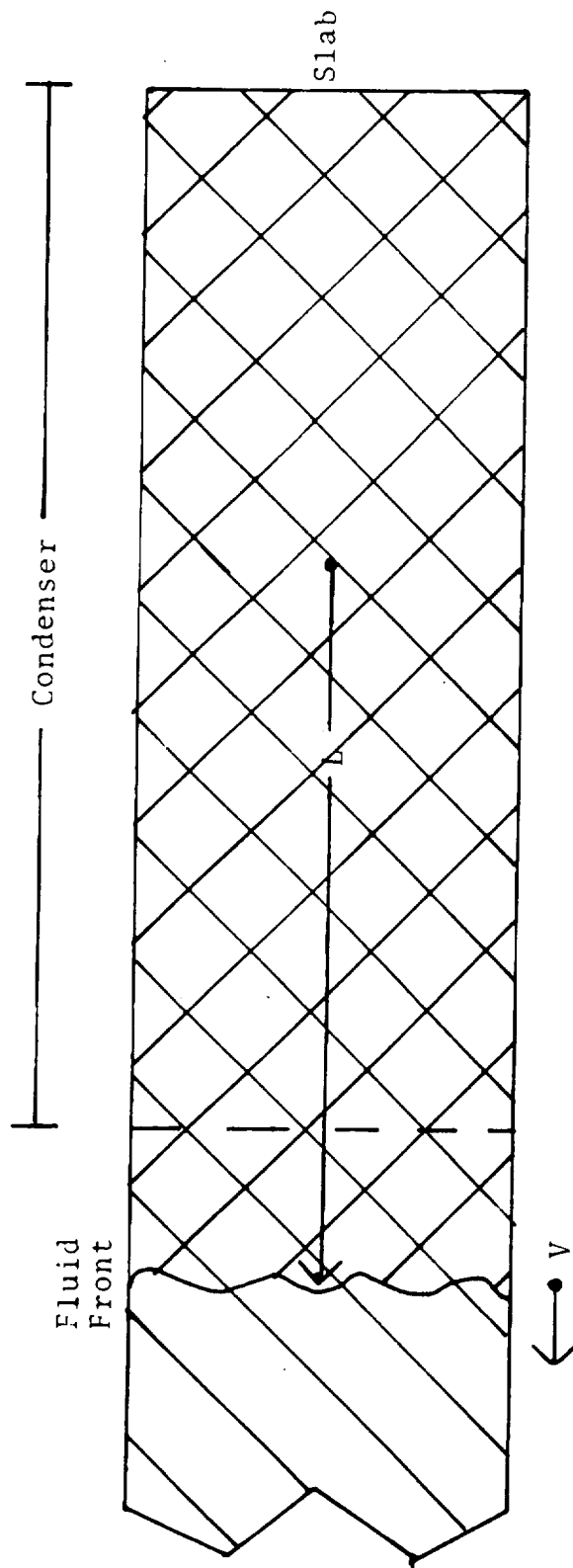


Figure 7. Model of Fluid Flow in Slab

$$V(t) = \frac{2\sigma_{\ell}}{\bar{K}\mu_{\ell}r_pL} \left(1 - e^{-\left(\bar{K} \frac{\mu_{\ell}}{\rho_{\ell}}\right)t}\right) \quad (3.2)$$

From this expression it can be seen that the time required for the fluid to reach a steady state velocity in an initially wetted capillary structure is a function of viscosity, inverse permeability, and density. For the particular heat pipe under study the fluid velocity reaches better than ninety percent of its steady state value in less than 0.05 seconds. Although this model is no doubt over simplified it does show that fluid velocities do develop very rapidly and would present no problem to startup in this heat pipe.

Velocity in the slab can be used to predict the capillary limited heat transfer rate with

$$Q_{cap} = \rho_{\ell} V A_c h_{fg} \quad (3.3)$$

Heat transfer from the evaporator can be limited to this value by restricting the number of nodes interacting with the vapor region.

In simulating startup from the supercritical an expression must be developed to predict the location of the fluid as it is pumped back towards the evaporator. Assume uniform and rapid condensation over the entire condenser surface when the temperature drops below the critical value.

Equation (3.1) can be solved explicitly in finite difference form:

$$V^{n+1} = \frac{\Delta t}{L^n} \left(\frac{2\sigma_\ell}{r_p \rho_\ell} - \bar{K} \frac{\mu_L^n V^n}{\rho_\ell} - V^{n^2} \right) + V^n \quad (3.4)$$

The length in equation (3.4) is allowed to vary with time as the fluid moves along the slab. The location of the fluid can be calculated from:

$$L = \int_0^t V \, dt \quad (3.5)$$

or in finite differences:

$$L^{n+1} = L^n + V^{n+1} \Delta t \quad (3.6)$$

An initial condition is needed for each equation. The initial velocity is assumed to be zero and the initial length is assumed to be one half the length of the condenser, measured from the midpoint of the condenser.

This length L , the distance from the center of the condenser to the fluid front, is used to calculate the node through which the fluid is currently moving. All nodes containing fluid are coupled with the vapor region. Those nodes still without fluid are insulated from the vapor. This manipulation of boundary conditions, made possible through

the use of the tridiagonal subroutine, permits any combination of nodes in the evaporator or condenser to actively working with or insulated from the vapor region.

D. Logic of Solution

The preceding equations were solved simultaneously on a Control Data Corporation Cyber-74 computer. A flow chart outlining the solution procedure is shown in Figure 8. The computer program is listed in Appendix D.

After reading dimensions and initial conditions a subroutine is called that calculates the properties and coefficients for each equation. The time steps are then started, each step requiring one pass through the program. Each of the equations is solved in a subroutine.

For each time step the new values of the vapor region and the heat sink temperatures are calculated first. These solutions are explicit and use evaporator and condenser values from the last time step. The new temperatures of the vapor and heat sink are then used as boundary conditions in the implicit solution of the evaporator and condenser system of equations.

The same subroutine that solves for a new vapor temperature also calculates the position of the fluid in the slab and determines which nodes in the evaporator and condenser are currently active. Because the vapor solution is explicit and has little mass it tends to become unstable.

Reproduced from
best available copy.

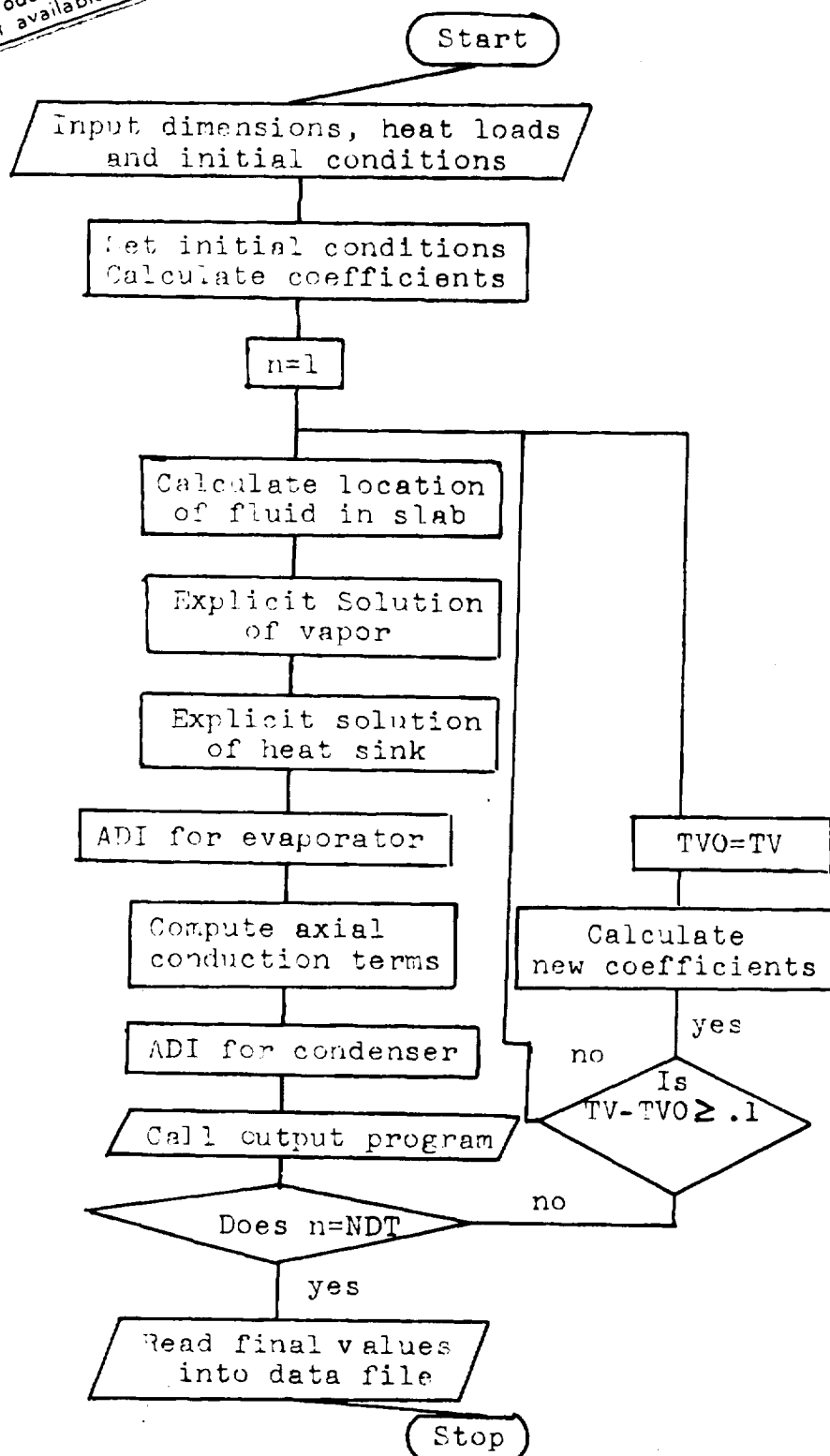


Figure 8. Flow Diagram of Computer Program

A discussion of stability is presented in Appendix E. This unstable tendency is overcome by allowing the program to calculate a smaller time step for the vapor region and iterate a sufficient number of times to complete the total time step.

The equation for the heat sink is solved in a separate subroutine. This routine can handle either a radiating heat sink or a cooling jacket. The solution is explicit but the mass is sufficiently large that stability is no problem.

Both the evaporator and condenser matrices are solved separately in the same subroutine. Inputs to the subroutine are temperatures at each node, coefficients, and boundary conditions. The subroutine calls the tridiagonal subroutine for solution of each row of the matrix. This technique is described in detail in references [16, 17, 18].

After each time step several checks are made. The current vapor temperature is compared to temperature used for calculation of property values. If the new value is different from the old by more than 0.1 K new coefficients are calculated using properties calculated at the new temperature.

Another check is performed to determine if the system is changing rapidly. If the system is changing temperature at a rate less than that specified the time step is doubled and new coefficients are calculated. Thus several different time steps may be used during a single run. The response time of the vapor region is less than the time steps normally

used. This presents no problem since inherent in the solution technique is the assumption that the system response is linear across a single time step. Thus the vapor temperature merely tracks the temperature changes in the evaporator and condenser sections. However when the time step is changed the vapor response is solved explicitly with evaporator and condenser temperatures calculated for the old value of the time step. The vapor temperature will then lag the rest of the solution by one half of a time step slowing down the response of the entire system. To correct for this problem the change in the vapor temperature is always multiplied by the ratio of the new time step to the old time step. In essence this procedure amounts to predicting the temperatures of the evaporator and condenser nodes that interact with the vapor for the new time step. Since this change of time step only occurs when the system is changing at a very slow rate any error that occurs would be small.

In startup from the supercritical the average specific heat of the slab changes as the fluid moves through it. Whenever the fluid reaches a new node the values are calculated again taking into account the additional fluid in the slab.

Values used for thermal conductivity of the wick are a weighted average of the thermal conductivities of the fluid and the screen. Effective thermal conductivity of the screen-fluid combination is evaluated using the method of Williams

[24]. Details of this development are in Appendix F.

Specific heats of the wick and slab are also weighted averages of the specific heats of the components.

E. Description of the Analog Model

A simplified model of the heat pipe was used for transient studies with an analog computer. This model assumed one dimensional conduction in the radial direction. Overall temperature drops and response times can be predicted with this technique for small perturbations.

The approach used for the analog computer was to break the heat pipe into nodes. A heat balance was written for each node equating the net heat gain with temperature increase. The result is a system of first order differential equations in time with temperature the dependent variable.

Since the computer capacity was limited only five nodes are used. Node 1 is composed of the outer half of the evaporator wall and is located at the evaporator surface. The inner half of the evaporator wall and the outer half of the wick make up node 2 which is located at the interface of the wick and wall. The vapor region, slab and adiabatic wall and wick are the components of node 3 located at the interface of wick and vapor region. Like node 2, node 5 is composed of one half of the wick and the inner half of the condenser wall and is located at the interface of condenser wick and wall. Node 6 is the outer half of the condenser

wall and like node 1 is located at the surface. Figure 9 is a schematic diagram of the nodes and their locations.

Equations for the six nodes are listed below. See Appendix G for a discussion of scaling the equations for use on the analog computer.

Condenser cooling is accomplished by means of a jacket with a circulating fluid. An additional node, number 6 permits the modeling of this jacket.

The analog computer circuit for these equations is shown in Figure 10.

$$\frac{dT_1}{dt} = \frac{4\pi \ell_E K_p}{\rho_p c_p v_{pE} \ln(r_o/r_B)} (T_2 - T_1) + \frac{2Q_E}{\rho_p c_p v_p} \quad (4.1)$$

$$\begin{aligned} \frac{dT_2}{dt} = & \frac{4\pi \ell_E K_p}{[\rho_p c_p v_{pE} + \rho_w c_w v_{wE}] \ln(r_o/r_B)} (T_1 - T_2) \\ & + \frac{4\pi \ell_E K_w}{[\rho_p c_p v_{pE} + \rho_w c_w v_{wE}] \ln(r_B/r_I)} (T_3 - T_2) \end{aligned} \quad (4.2)$$

$$\begin{aligned} \frac{dT_3}{dt} = & \frac{4\pi \ell_E K_w}{[\rho_p c_p v_{pE} + \rho_w c_w v_{wE} + m_a c_a] \ln(r_B/r_I)} (T_2 - T_3) \\ & + \frac{4\pi \ell_C K_w}{[\rho_p c_p v_{pC} + \rho_w c_w v_{wC} + m_a c_a] \ln(r_B/r_I)} (T_4 - T_3) \end{aligned} \quad (4.3)$$

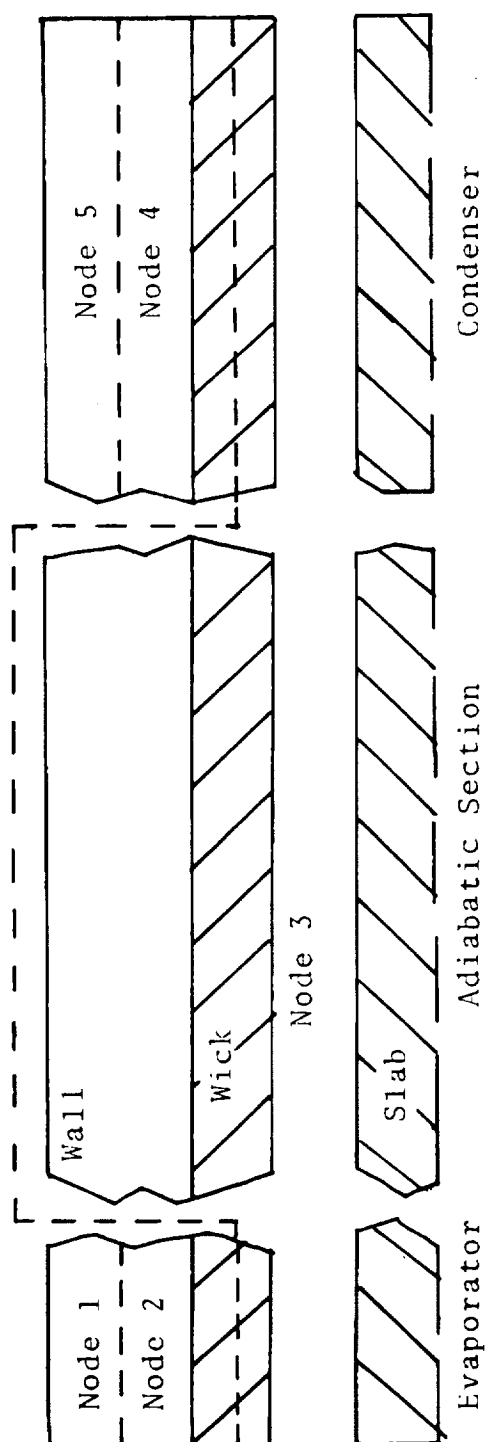


Figure 9. Schematic Diagram of Analog Model

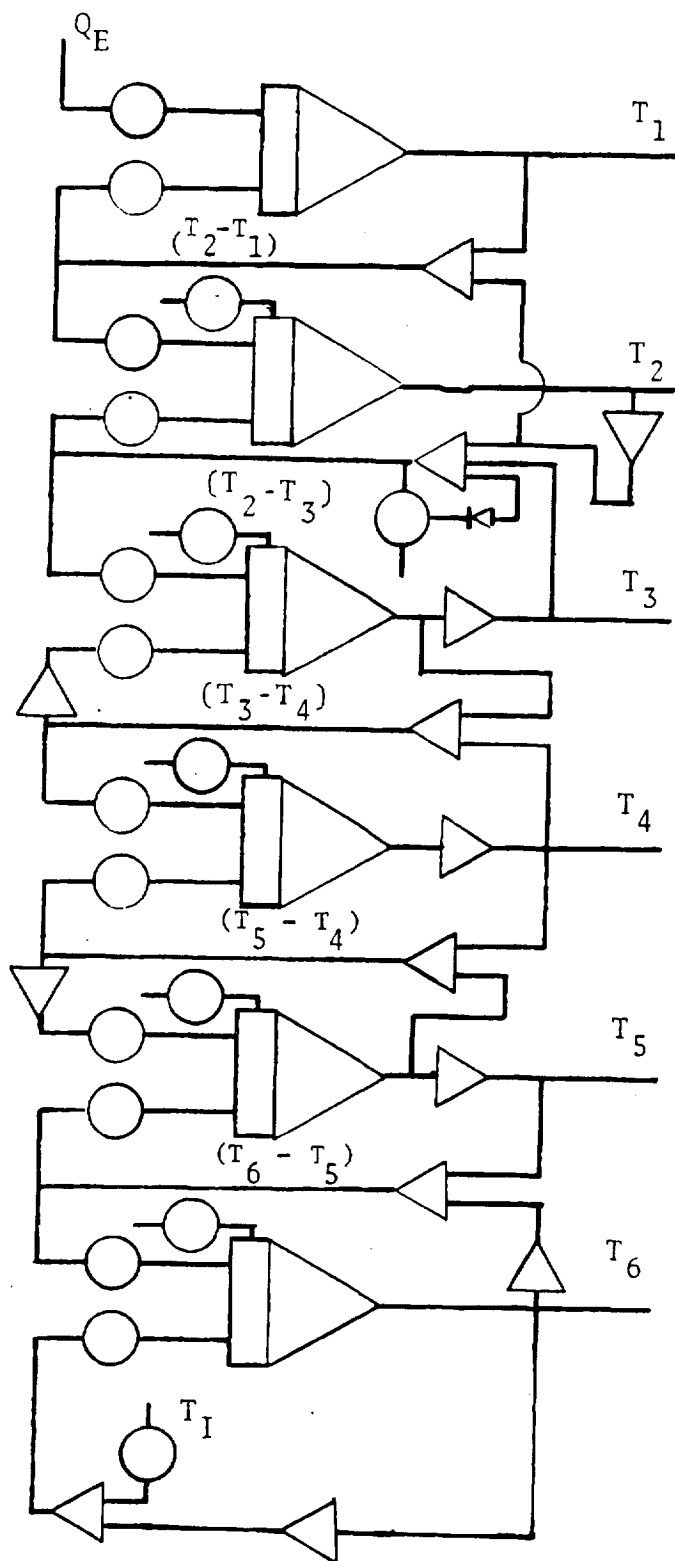


Figure 10. Analog Circuit

$$\begin{aligned} \frac{dT_4}{dt} = & \frac{4\pi \ell_C K_w}{[\rho_p c_p v_{pC} + \rho_w c_w v_{wC}] \ln(r_B/r_I)} (T_3 - T_4) \\ & + \frac{4\pi \ell_C K_p}{[\rho_p c_p v_{pC} + \rho_w c_w v_{wC}] \ln(r_O/r_B)} (T_5 - T_4) \end{aligned} \quad (4.4)$$

$$\begin{aligned} \frac{dT_5}{dt} = & \frac{4\pi \ell_C K_p}{\rho_p c_p v_{pC} \ln(r_O/r_B)} (T_4 - T_5) \\ & + \frac{4\pi r_O \ell_C h_C}{\rho_p c_p v_{pC}} (T_6 - T_5) \end{aligned} \quad (4.5)$$

$$\frac{dT_6}{dt} = \frac{2\pi r_O \ell_C h_C}{m_{CJ} c_{CJ}} (T_5 - T_6) + \frac{\dot{m}_f c_f}{m_{CJ} c_{CJ}} (T_I - T_6) \quad (4.6)$$

III. RESULTS AND COMPARISONS

The digital model has been used to model the heat pipe studied by Saaski [26]. The heat pipe modeled had an evaporator and condenser each 15.24 cm long and a 15.0 cm adiabatic section. Methanol was used for the working fluid. The inside radius was 1.288 cm and the wall thickness was 0.080 cm. One layer of 200 mesh screen was used as a circumferential wick. An air gap of 0.022 cm was maintained between the condenser surface and the heat sink for a per-unit-length gap conductance of approximately 0.0443 W/cm-K. The temperature of the vapor region is non-dimensionalized by defining

$$\frac{\Delta T_V}{\Delta T_{Vm}} = \frac{T_V(t) - T_{Vo}}{T_{Vm} - T_{Vo}}$$

where T_{Vo} is the initial vapor temperature and T_{Vm} is the steady state vapor temperature. Saaski's data reaches 95 percent of steady state values in approximately 130 seconds. The predicted curve using the technique of this study responds more slowly reaching 95 percent of steady state in 160 seconds. Both curves are shown in Figure 11.

The digital model of the heat pipe has been used to study three different cryogenic heat pipe systems. Systems

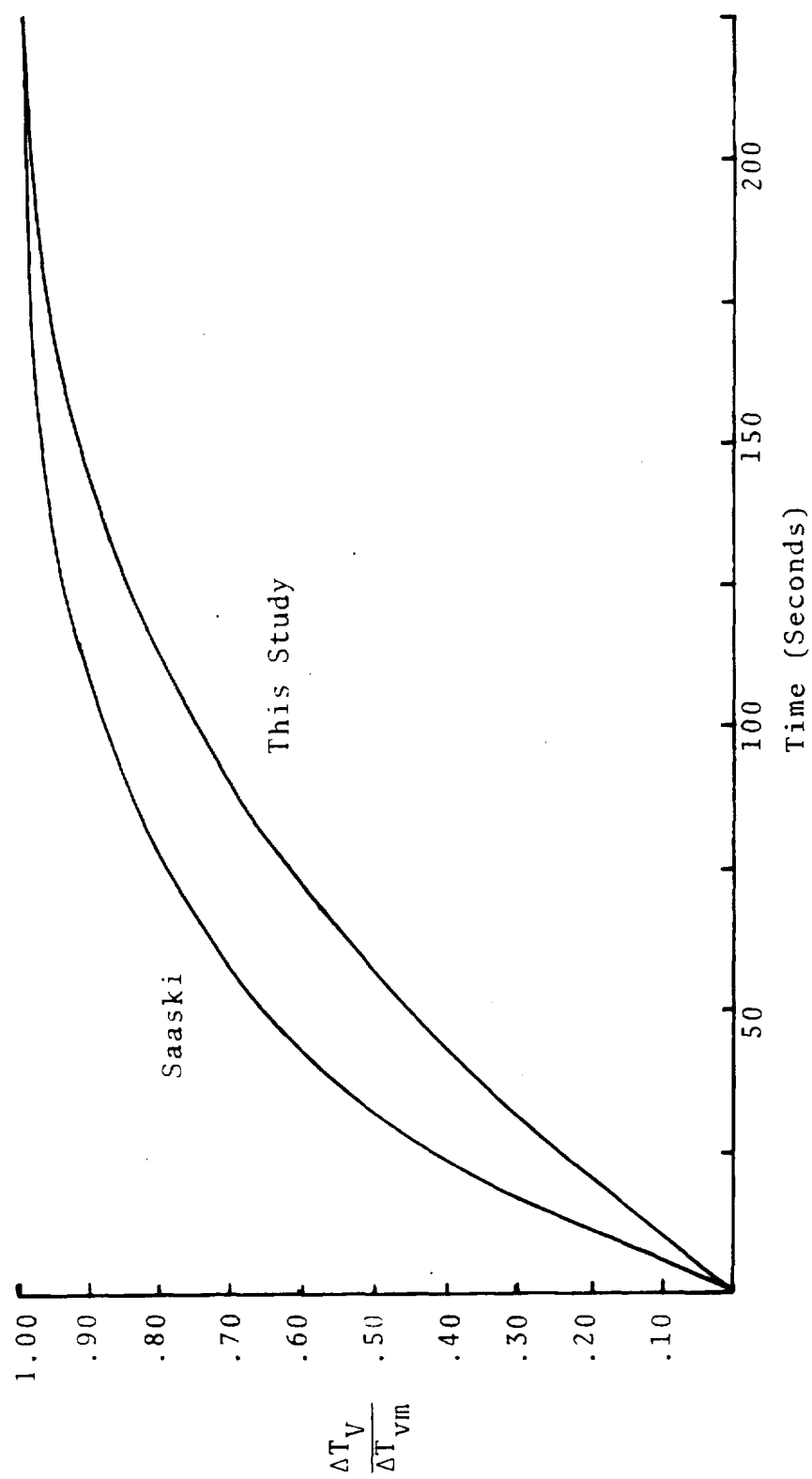


Figure 11. Comparison of Model with Experimental Data from the Literature

are varied by changing boundary conditions on the condenser surface. The effect of varying heat pipe design parameters was studied using a model with the condenser surface temperature fixed. Other systems modeled used a cooling jacket and a radiating surface as heat sinks.

Similar studies have been performed on the constant condenser temperature heat pipe and the cooling jacket using the analog model.

An even simpler model can be developed if the system is assumed to be a lumped mass. Details of this development for a heat pipe with a cooling jacket are given in Appendix H. The result is a simple exponential equation. This model should have a faster response than the more complex models, since no temperature gradient must develop. A comparison of digital, analog, and exponential models for startup from isothermal at 100 K to a heat load of 15 watts is shown in Figure 12. In each case the condenser heat sink is a cooling jacket with liquid nitrogen at 100 K as the coolant. All three models predict similar responses.

The digital model of a system with a constant condenser surface temperature was used to study effects of varying design parameters. In each case the heat pipe is initially isothermal at 100 K. A heat flux of 15 watts is imposed on the evaporator surface and the heat pipe adjusts to steady state. Table 2 lists the various cases studied.

Figure 13 compares analog and digital response curves

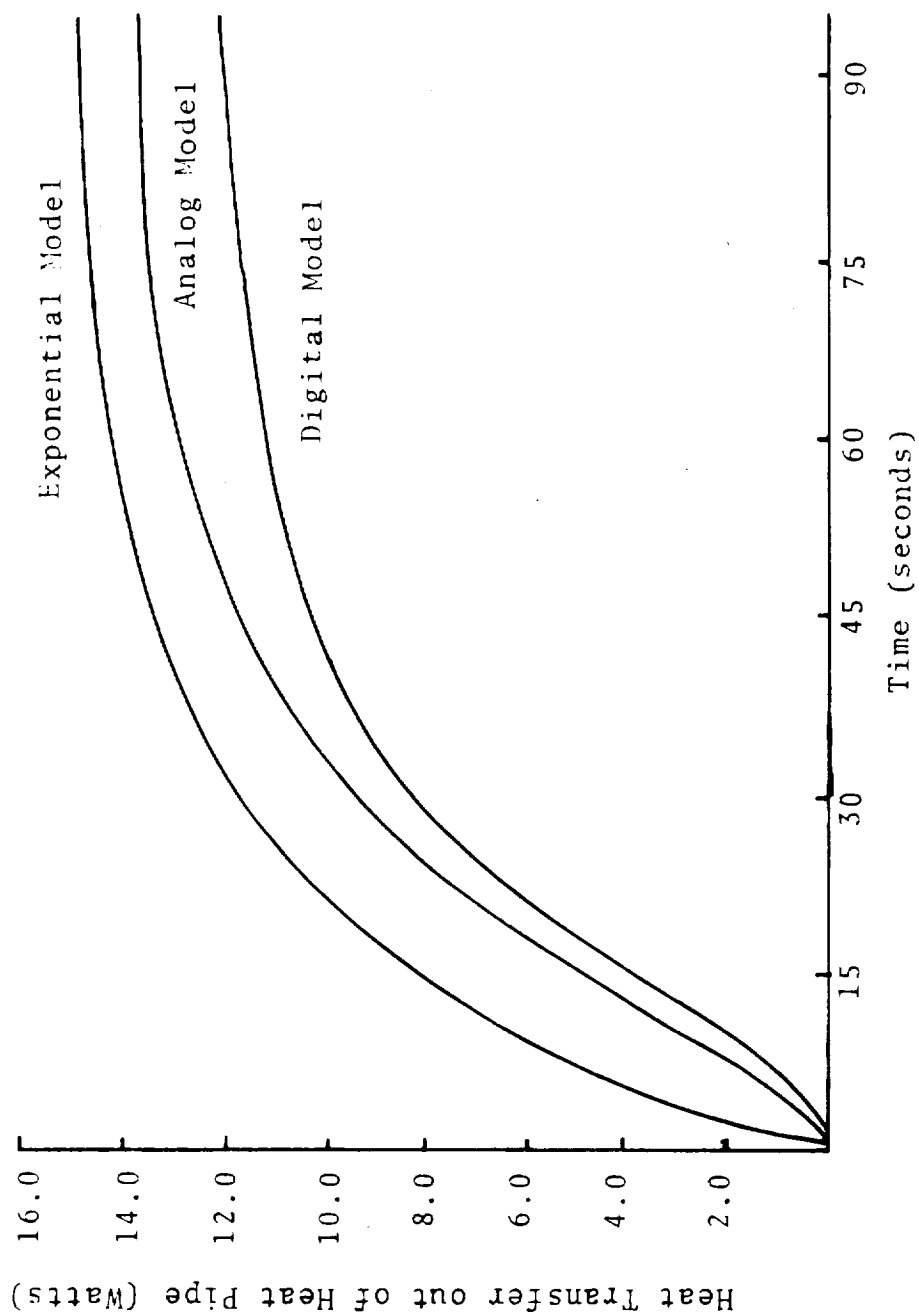


Figure 12. Comparison of Exponential, Analog, and Digital Models for Heat Pipe with Cooling Jacket

Table 2. Parameters for Cases Studied

Case No.	Modification
1	Standard Heat Pipe as described Table 1
2	Wall thickness .2030 cm
3	Wall thickness .4060 cm
4	Circumferential wick of 4 layers 400 mesh
5	Circumferential wick of 8 layers 400 mesh
6	Fluid gap .006096 cm
7	Fluid gap .012192 cm
8	Slab 2 layers 400 mesh 2 layers 30 mesh
9	Slab 8 layers 400 mesh 10 layers 30 mesh

In each case the heat pipe is initially isothermal at 100 K. A heat flux of 15 watts is imposed on the evaporator surface. The only modification from the heat pipe of Table 1 is that listed.

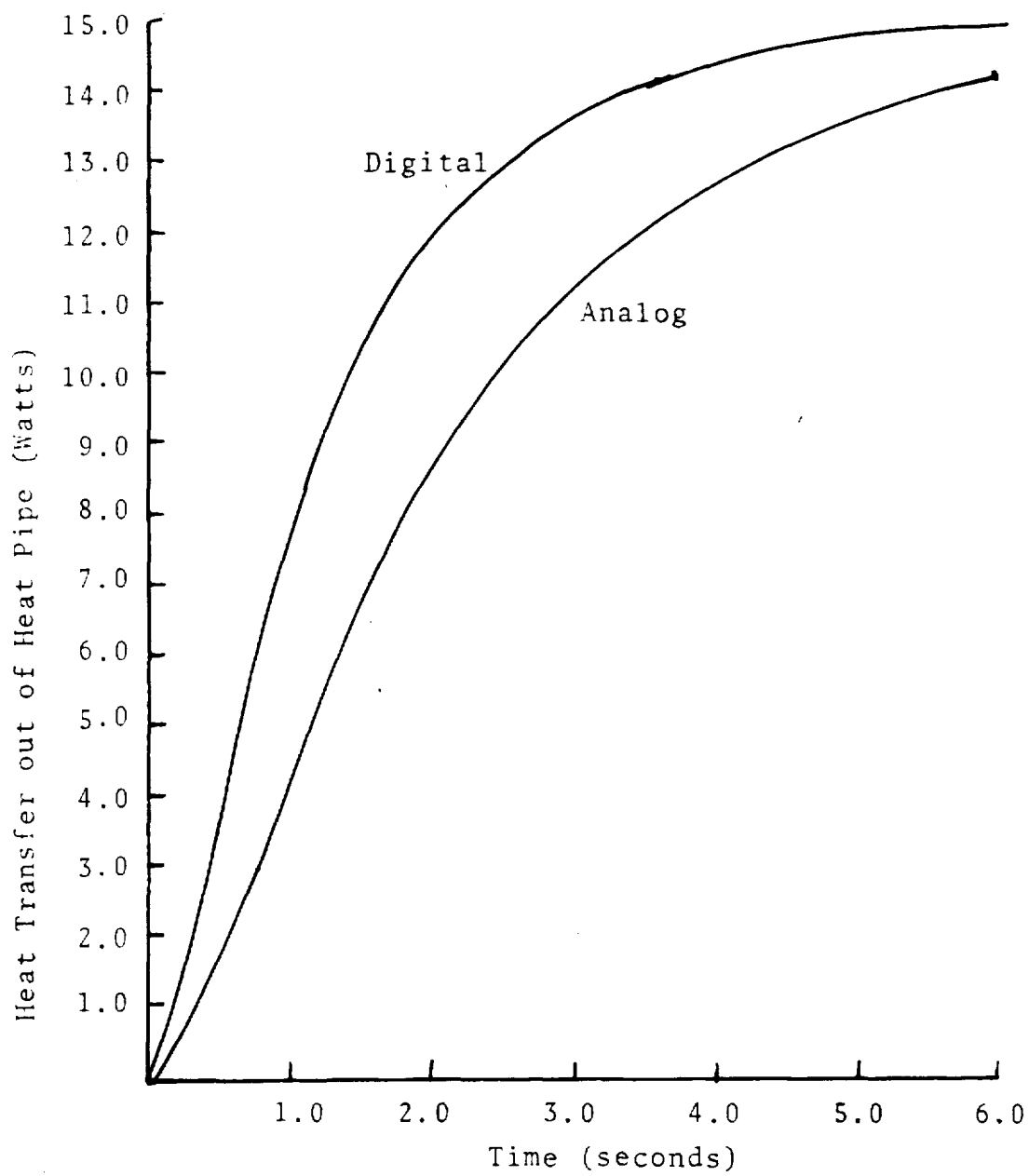


Figure 13. Comparison of Analog and Digital Model for Case 1

for case 1. The slower response of the analog curve is due to the different nature of the nodal systems employed.

The effect of changing the wall thickness is shown in Figure 14. Since the pipe wall is the major portion of the heat pipe mass, any change would have a great effect on heat pipe response. The pipe wall is also the largest thermal resistance in the heat pipe. Thus increasing the wall thickness requires a larger overall temperature difference. The time required for this temperature profile to develop slows response.

Increasing the number of layers of circumferential wick also increases the steady state temperature drop from evaporator to condenser. This effect as well as the added mass slow response as shown in Figure 15.

Figures 16 and 17 show the effect of changing the size of the fluid gap and the configuration of the composite slab. As the curves show the change in response time is very small.

Due to the nature of the model the response takes the same time for any heat input. Figure 18 shows the response for a heat input of 5 watts and 15 watts. Also shown is the response of a heat pipe to a power change from 5 to 15 watts. Each curve is for a heat pipe with a constant temperature condenser. In all three cases 95 percent of total change is achieved at the same time.

The thermal properties used in the model vary with temperature. The effect of this phenomena on response is

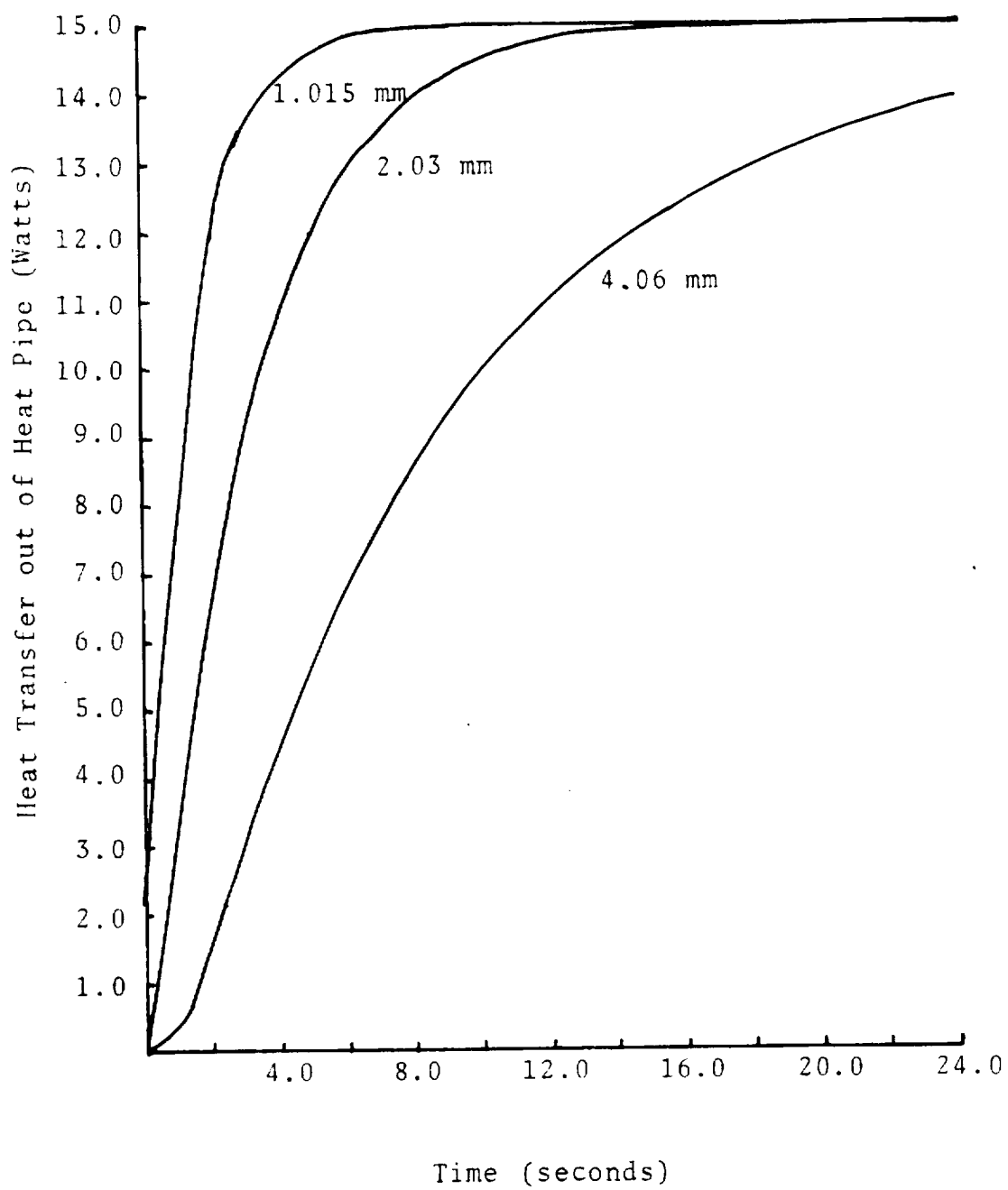


Figure 14. Effect of Changing Wall Thickness

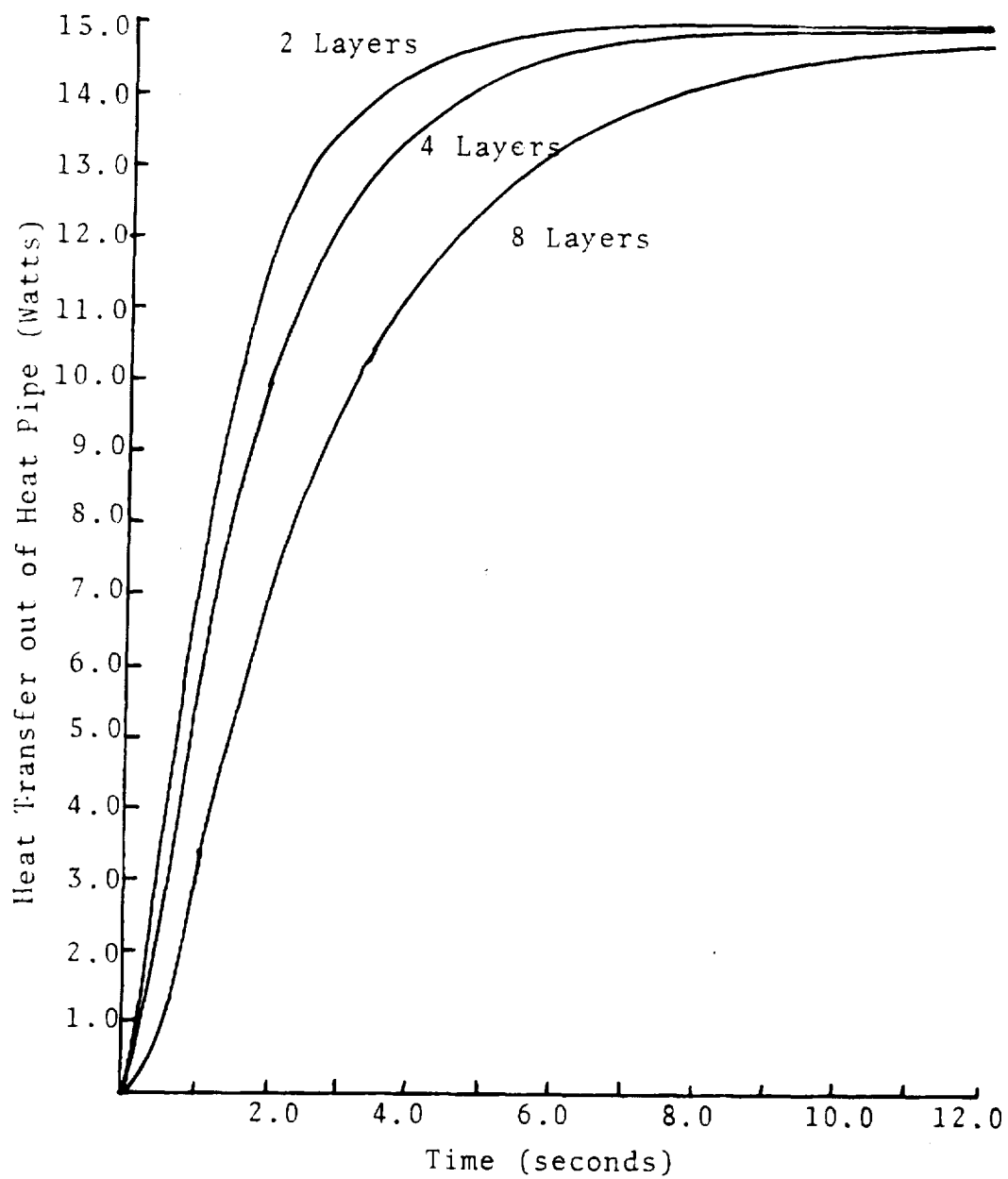


Figure 15. Effect of Changing Number of Wick Layers

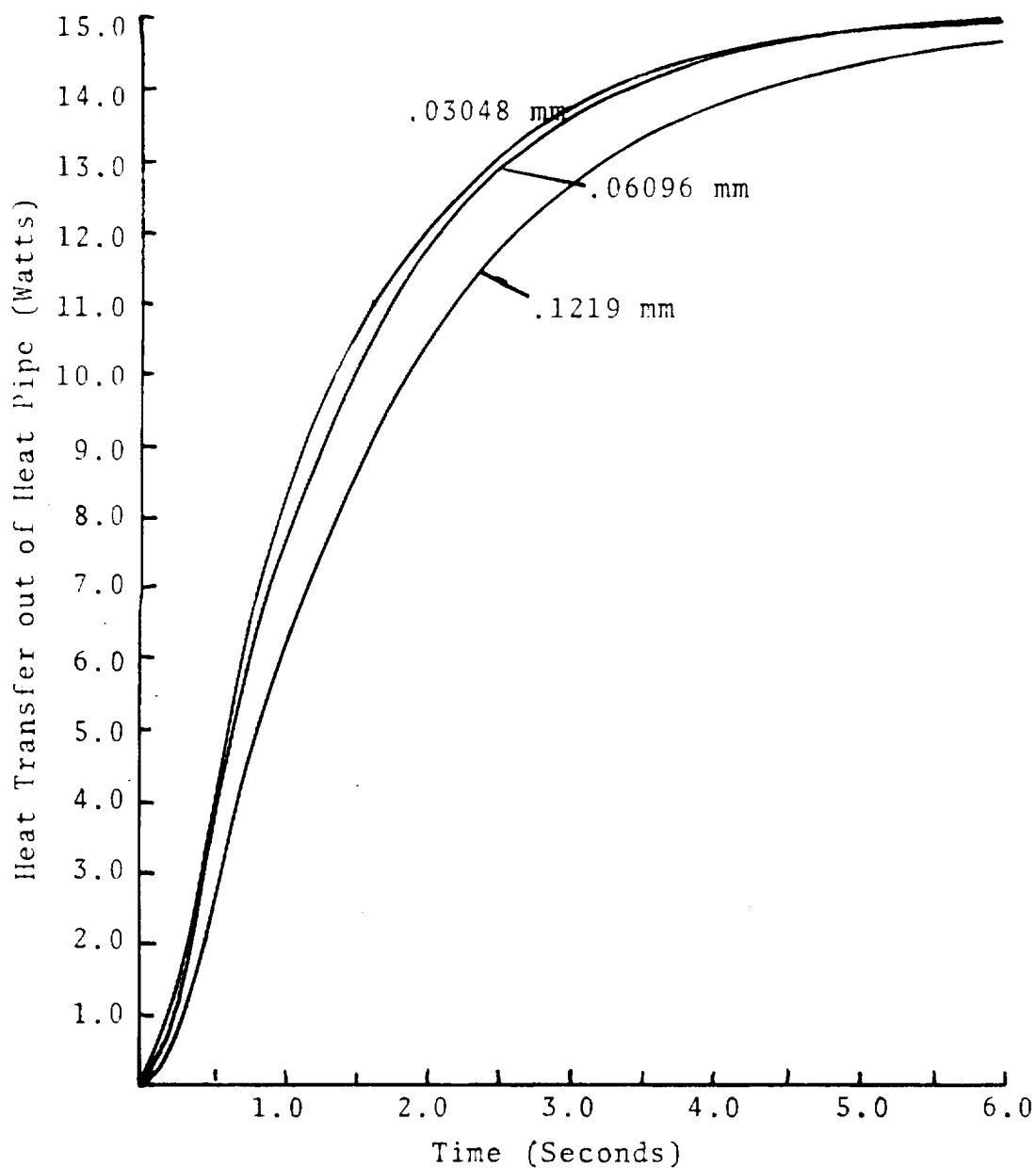


Figure 16. Effect of Changing Thickness of Fluid Gap

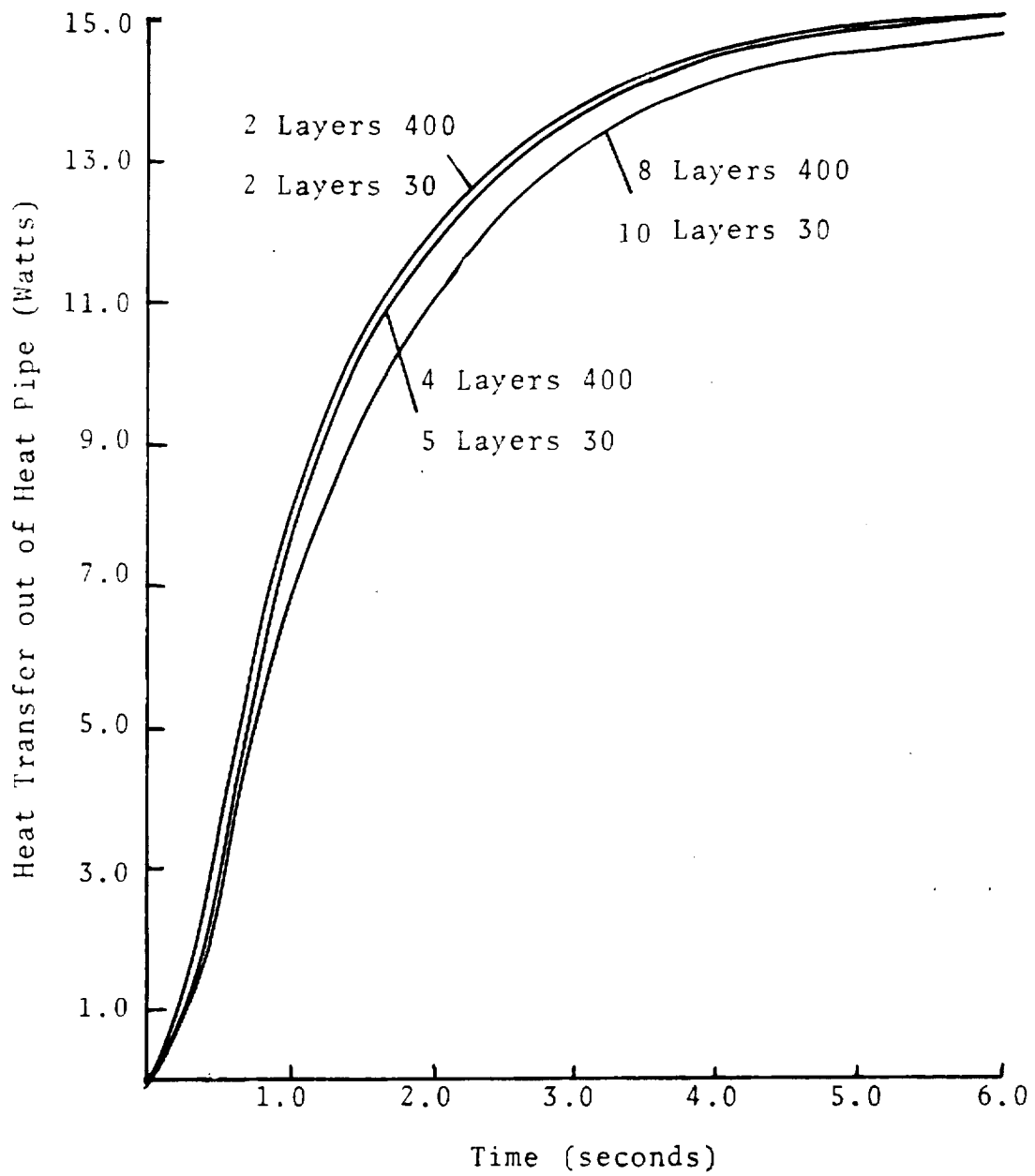


Figure 17. Effect of Changing Slab Composition

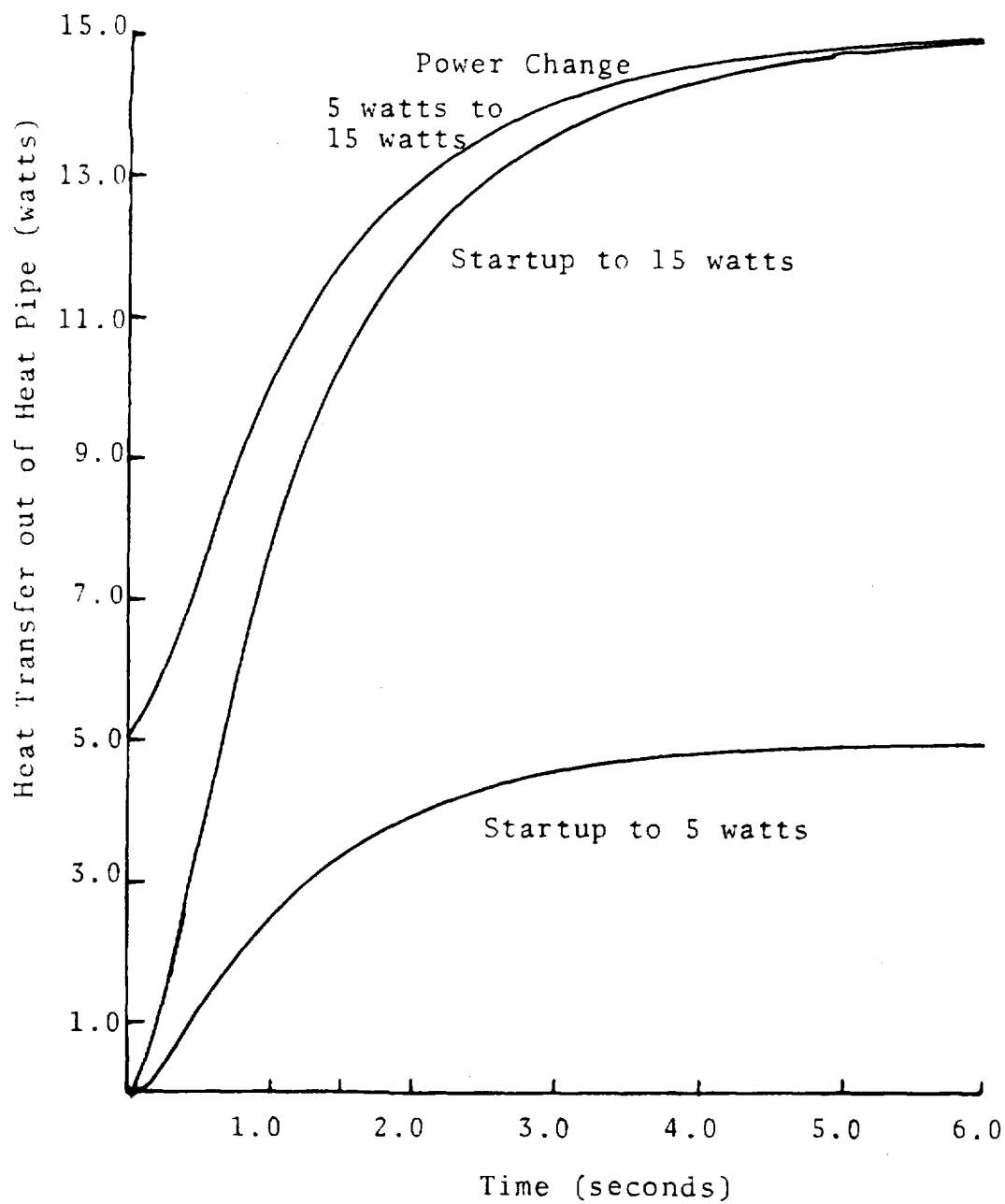


Figure 18. Comparison of Startup at Different Power Levels

shown in Figure 19. All three cases show an initially isothermal heat pipe with a constant condenser surface temperature. A heat flux of 15 watts is imposed on the evaporator. Curves are shown for startup from 80, 100, and 120 K. At the lower temperature the specific heats are smaller and the response is faster. At 120 K the capillary limitation is less than 15 watts. The effect of capillary limitation is also shown in Figure 19. The development of the overall temperature difference is shown in Figure 20. Note that at 120 K capillary burnout causes evaporator temperature to increase rapidly.

A heat pipe system with a cooling jacket and one with a radiating surface are compared in Figures 21 and 22. Since the heat leaving the radiating surface is dependent on the temperature alone the response time is much greater. This demonstrates the phenomena of temperature choking referred to by Anand, et al. [13].

Startup from the supercritical is shown in Figure 23. A heat flux of 5 watts is imposed on a heat pipe initially isothermal at 130 K. Cooling is imposed at the same time with a jacket with a coolant at 100 K and a surface coefficient of $1000 \text{ W/m}^2\text{-K}$. The evaporator surface temperature climbs sharply until fluid reaches it. The temperature falls rapidly and the heat pipe begins working.

Figure 24 compares wicking velocity calculated using equations 3.4 and 3.6 with velocities from the work of Symons

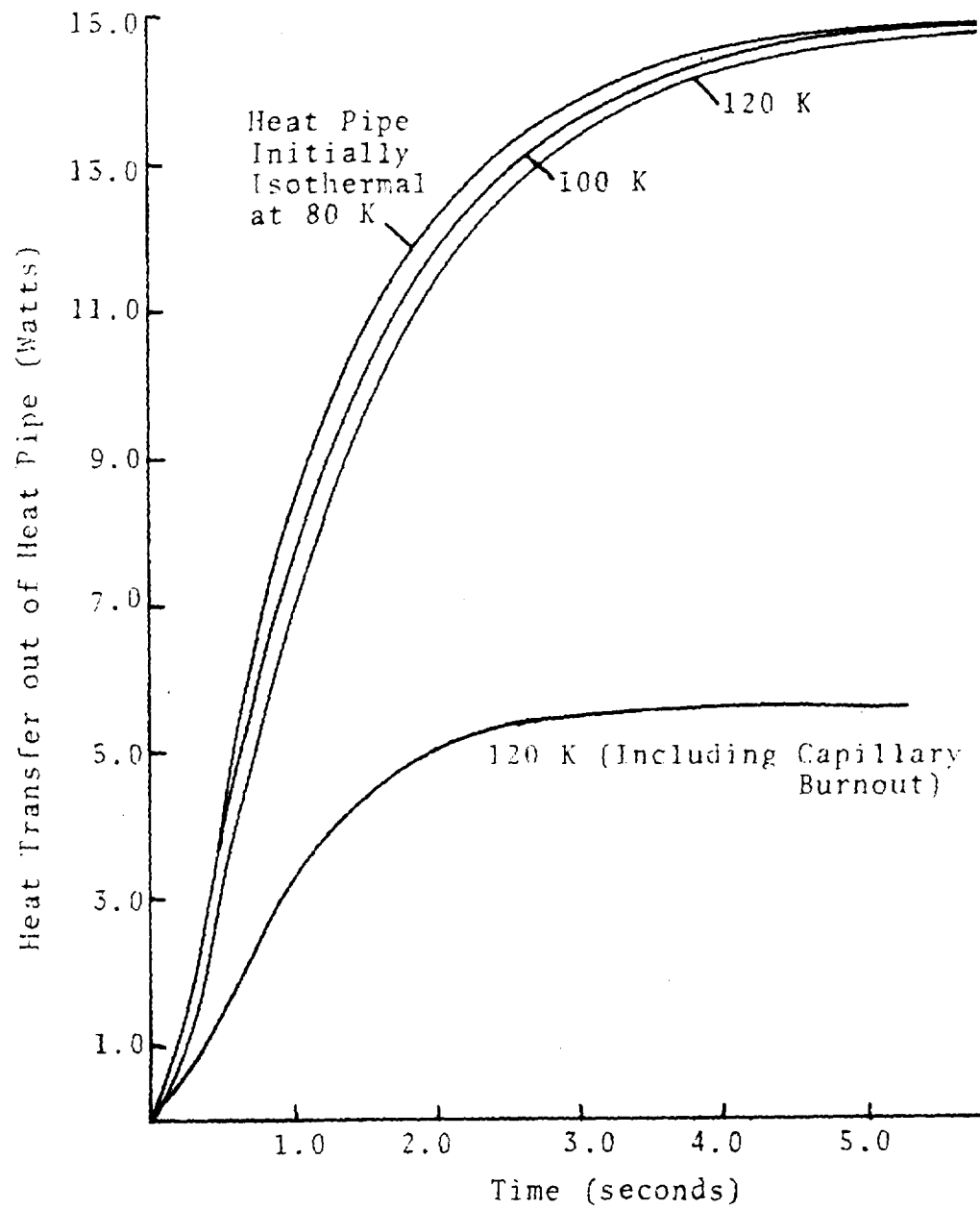


Figure 19. Comparison of Startup at Different Temperatures

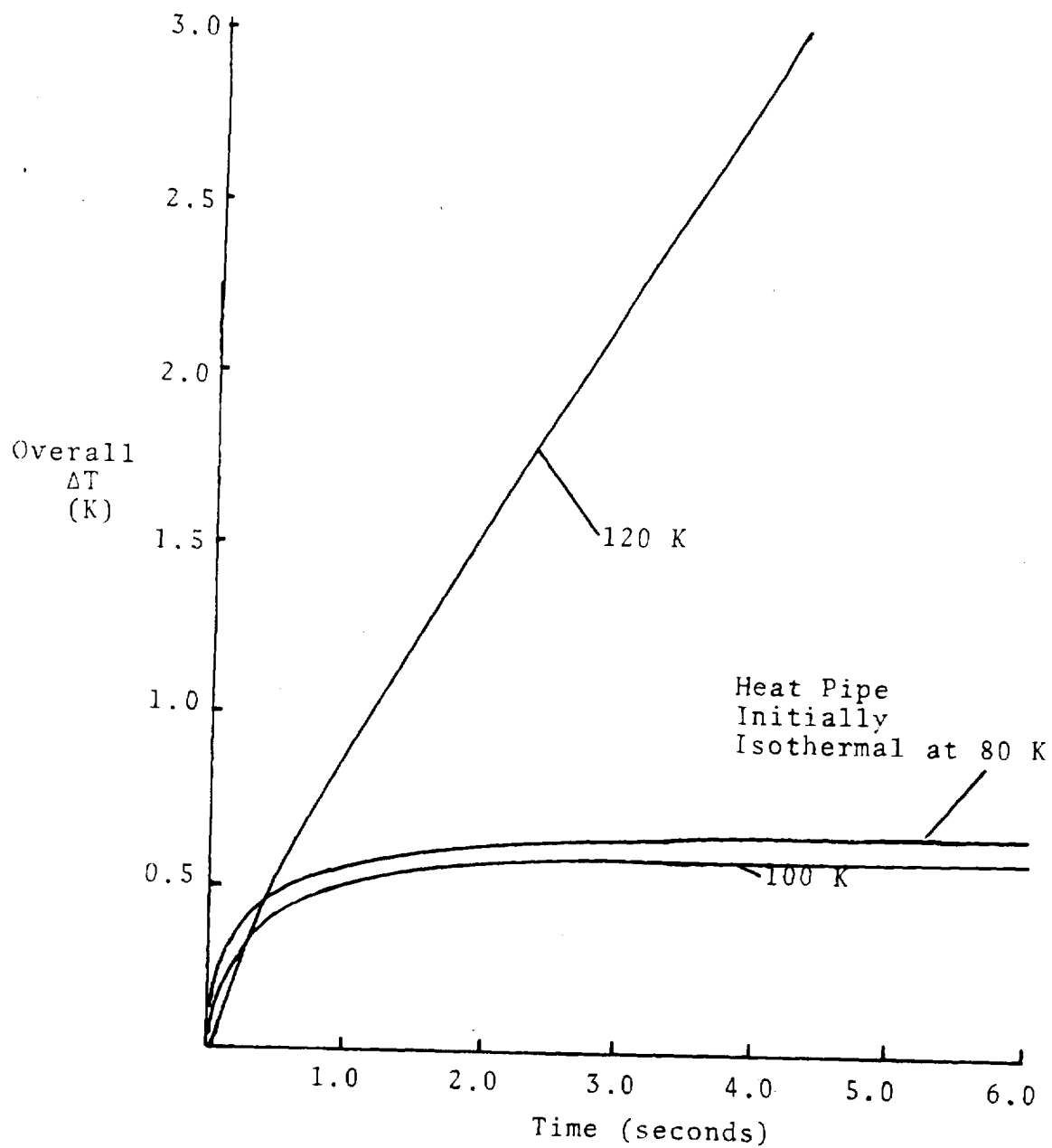


Figure 20. Development of Overall Temperature Gradients

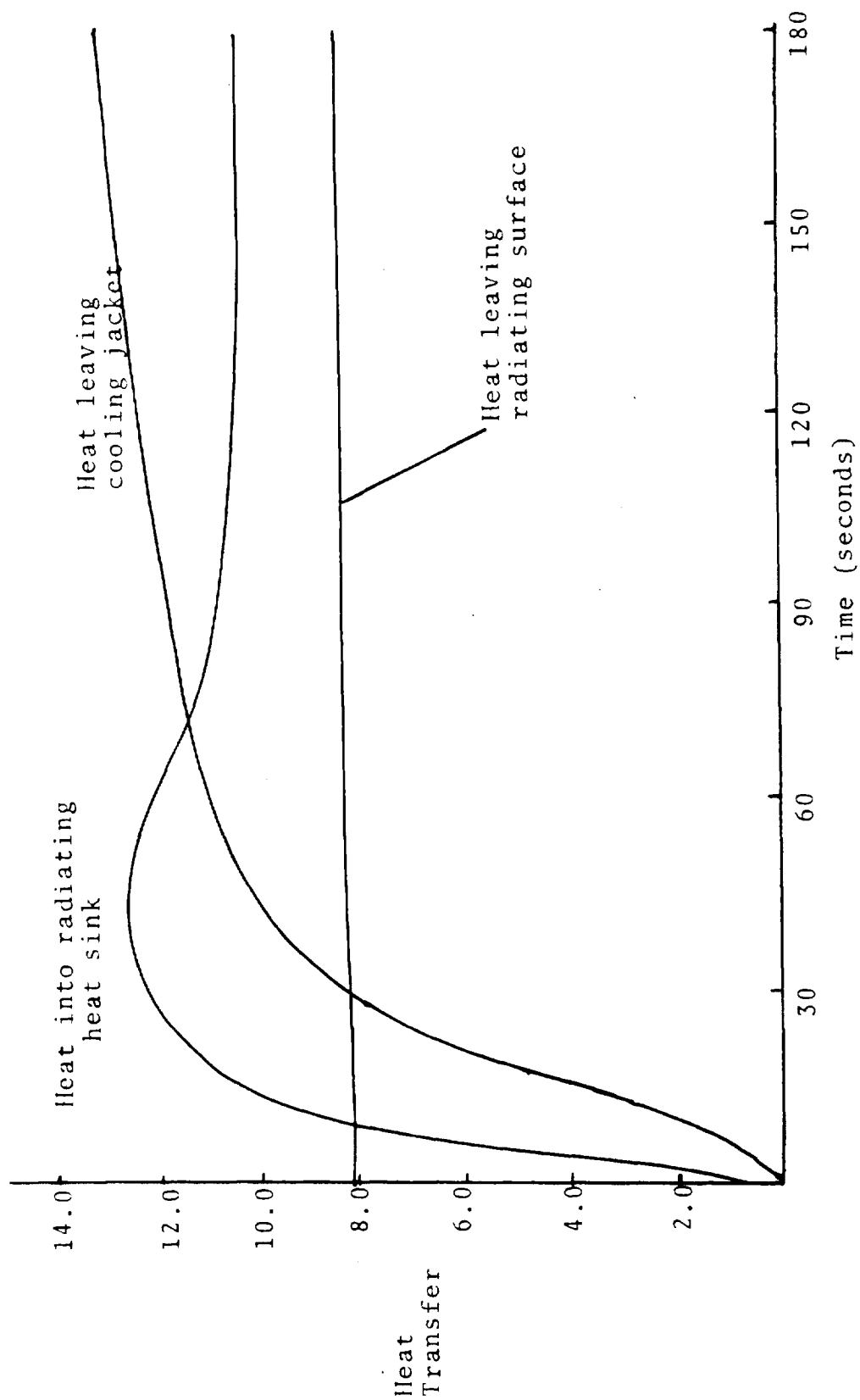


Figure 21. Comparison of Heat Pipe Response with Cooling Jacket or Radiating Surface Heat Sink

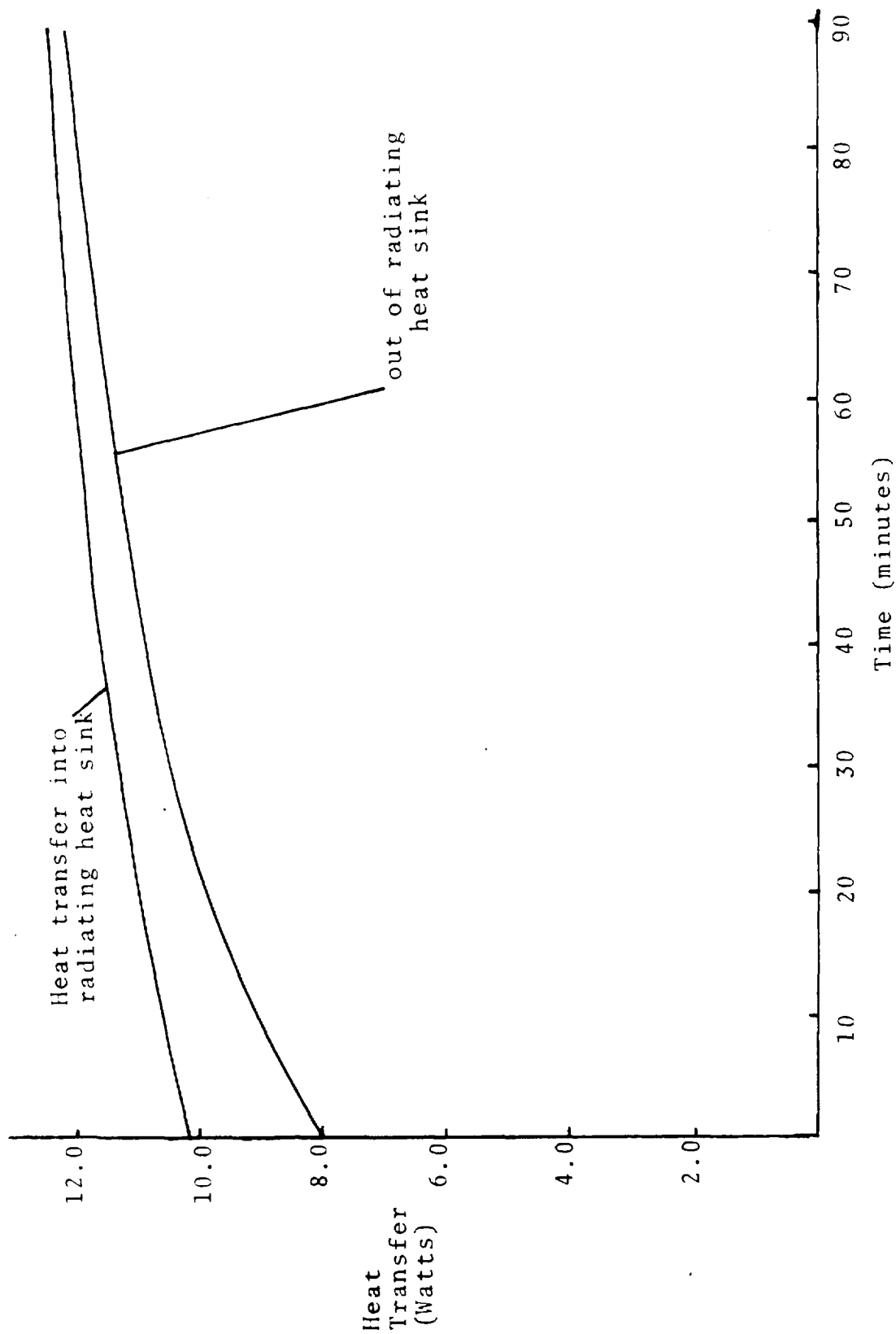


Figure 22. Response of Radiating Heat Sink

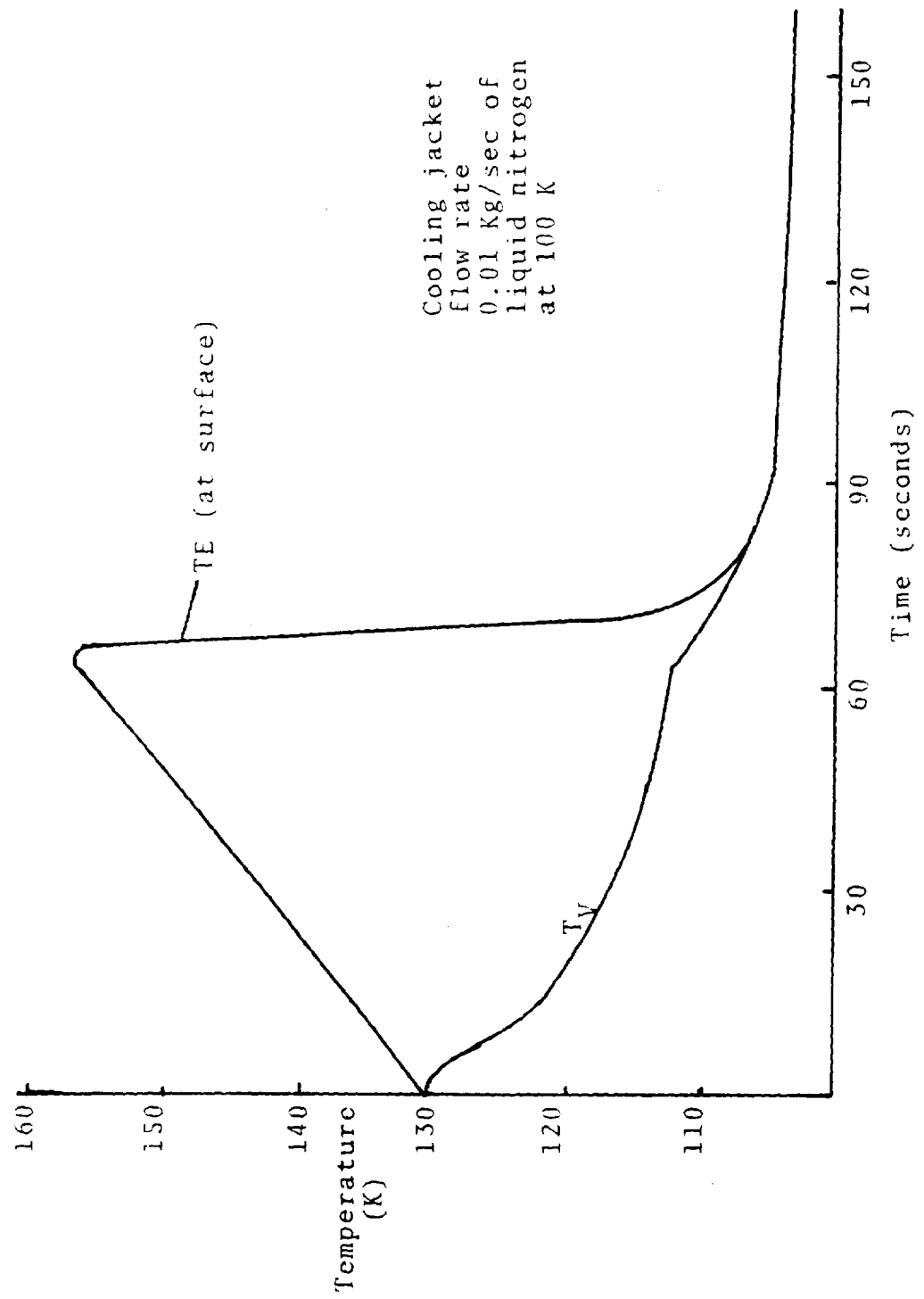


Figure 23. Startup from Supercritical

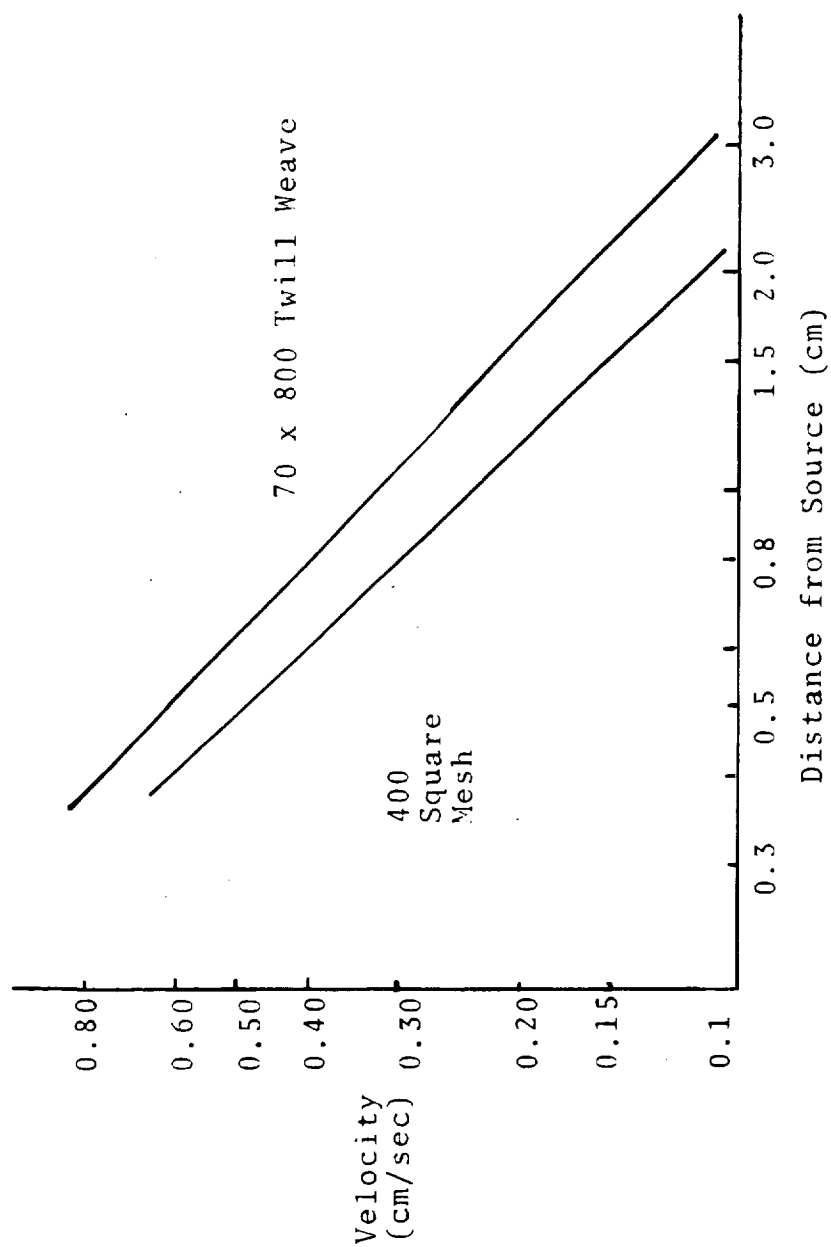


Figure 24. Comparison of Predicted Fluid Velocity with Data from Literature

[27]. For both curves the working fluid is methanol. Since the capillary structures are not the same the velocities do not agree exactly. However they are of the same order of magnitude.

Wicking velocity in the composite slab is shown in Figure 25. The velocities are much larger than those of Figure 24 because of the nature of the composite slab. The effective inverse permeability is relatively small due to the presence of the 30 mesh screen yet the pumping pressure is relatively high due to the outer layers of 400 mesh screen.

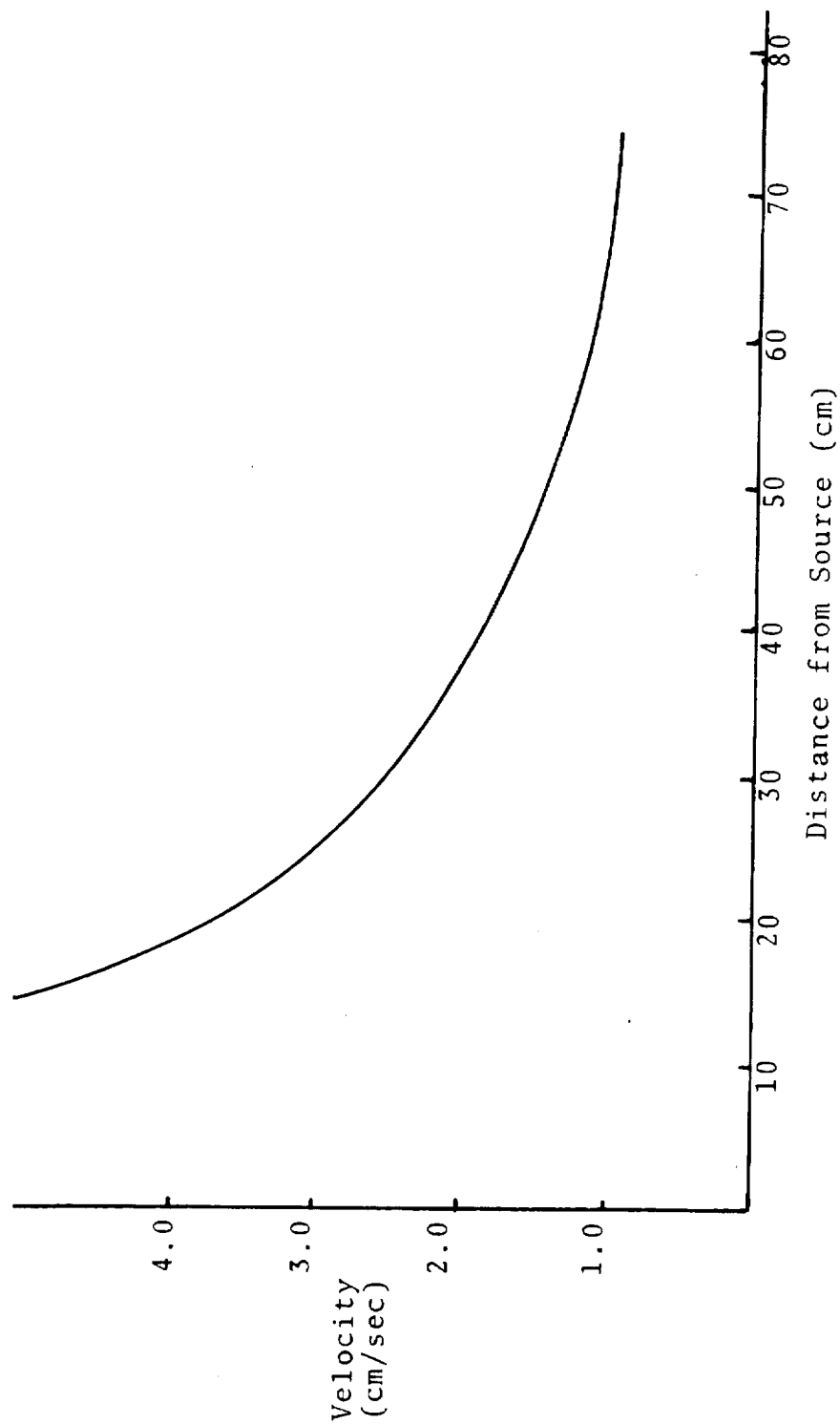


Figure 25. Velocity with Position in Composite Slab

IV. CONCLUSIONS AND RECOMMENDATIONS

This study has developed a technique for predicting transient response of heat pipes. Predicted response curves were compared with experimental data from the literature and agreement was good. Results from the digital studies have been compared with those from more simple analog and exponential models and trends are found to be similar.

The analog model provides a good method for estimating response for small transients. Because of the large node spacing and assumption of constant property values the results are not as accurate as the digital model and the effects of fluid dynamics and startup from the supercritical could not be included. An attempt to improve the analog model would have required more analog computing capability than was available.

A much better technique for modeling transients is provided by the digital model. Thermal properties are allowed to vary with temperature and the effects of fluid dynamics are included. It was found that in accurately modeling experimental data it was difficult to account for response times of heating and cooling systems and the added masses of instrumentation and insulation. A simple approach was developed for including

startup from the supercritical.

The stability of the alternating direction implicit solution procedure was found to be very good. (See Appendix E for a discussion of stability.) The program remained stable for time steps as large as thirty seconds. Had an explicit solution of the same node system been attempted, time steps on the order of 10^{-3} seconds would have been necessary to maintain stability. With the ADI method some oscillations would occur near the boundaries when the time steps were large and the system was changing temperature rapidly.

In any continuation of this work many improvements could be made in the computer code to decrease running time. In addition the equations which are used to predict wick re-priming after dryout could be improved.

APPENDICES

APPENDIX A

TRANSFORMATION OF COORDINATE SYSTEMS

It is convenient to transform the cylindrical coordinate system that describes the heat pipe to one that is rectangular. In cylindrical coordinates $\nabla^2 T$ is

$$\frac{\partial^2 T}{\partial r^2} + \frac{1}{r} \frac{\partial T}{\partial r} + \frac{1}{r} \frac{\partial^2 T}{\partial \phi^2} + \frac{\partial^2 T}{\partial z^2}$$

Make the following substitutions

$$x = \ln(r_0/r_I)$$

$$y = \phi$$

$$z = z$$

Thus

$$\frac{\partial^2 T}{\partial r^2} = \frac{\partial}{\partial r} \left(\frac{1}{r} \frac{\partial T}{\partial x} \right) = \frac{\partial^2 T}{\partial x^2} \frac{1}{r^2} - \frac{1}{r^2} \frac{\partial T}{\partial x}$$

$$\frac{\partial^2 T}{\partial \phi^2} = \frac{\partial^2 T}{\partial y^2}$$

$$\frac{\partial^2 T}{\partial z^2} = \frac{\partial^2 T}{\partial z^2}$$

Substitution back into $\bar{\nabla}^2 T$

$$\frac{1}{r^2} \frac{\partial^2 T}{\partial x^2} - \frac{1}{r^2} \frac{\partial T}{\partial x} + \frac{1}{r^2} \frac{\partial T}{\partial x} + \frac{1}{r^2} \frac{\partial^2 T}{\partial y^2} + \frac{\partial^2 T}{\partial z^2}$$

or

$$\frac{1}{r^2} \frac{\partial^2 T}{\partial x^2} + \frac{1}{r^2} \frac{\partial^2 T}{\partial y^2} + \frac{\partial^2 T}{\partial z^2}$$

This transformation simplifies calculation and makes finite difference approximation of the equations easier. Figure 26 shows the result of this transformation.

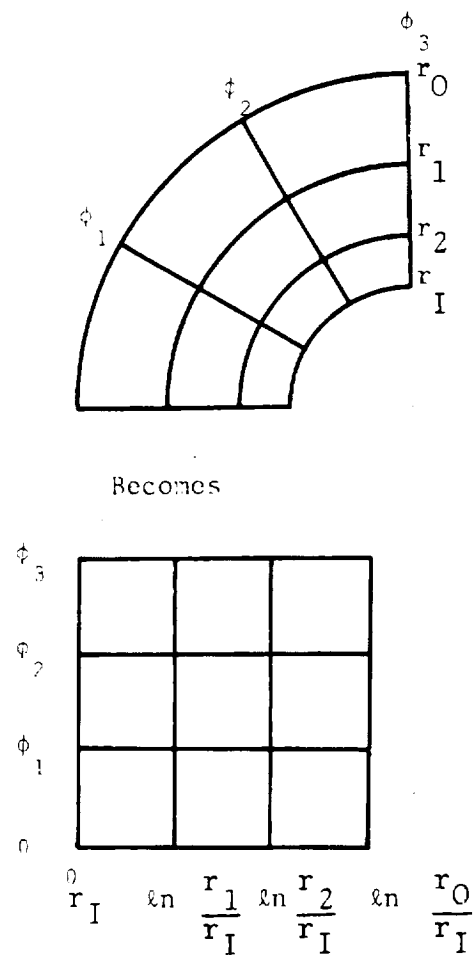


Figure 26. Polar to Rectangular Transformation

APPENDIX B

THERMODYNAMIC PROPERTY EQUATIONS

In his thesis Hare [8] developed polynomial expressions for the thermal properties of nitrogen and stainless steel as a function of temperature. A least squares regression analysis program on a Wang 720 calculator was used. These equations have been converted to International units and are presented here. Expressions for the specific heats of nitrogen, stainless steel and aluminum were developed using the same technique and data from references [23,25].

T = temperature in degrees Kelvin

Properties of liquid nitrogen

Density (Kg/m^3)

$$\begin{aligned} \rho_\ell = & -5.7784 \times 10^{-10} T^7 + 2.45356 \times 10^{-7} T^6 - 3.49017 \times 10^{-5} T^5 \\ & + 8.3300 \times 10^{-4} T^4 + 2.7794 \times 10^{-1} T^3 - 3.10677 \times 10 T^2 \\ & + 1.31038 \times 10^3 T - 1.94571 \times 10^4 \end{aligned}$$

Viscosity (N-sec/m^2)

$$\begin{aligned} \mu_\ell = & -2.25319 \times 10^{-11} T^4 + 6.541176 \times 10^{-9} T^3 - 5.51203 \times 10^{-7} T^2 \\ & + 2.708099 \times 10^{-6} T + 1.0352966 \times 10^{-3} \end{aligned}$$

Surface tension (N/m)

$$\begin{aligned} \sigma_\ell = & 1.026812 \times 10^{-9} T^4 - 3.919365 \times 10^{-7} T^3 + 5.631364 \times 10^{-5} T^2 \\ & - 3.804096 \times 10^{-3} T + 1.1066907 \times 10^{-1} \end{aligned}$$

Heat of vaporization (J/Kg)

$$h_{fg} = - 3.25198085 \times 10^{-6} T^6 + 9.1831855 \times 10^{-4} T^5 \\ - 3.4922526 \times 10^{-2} T^4 - 1.3994675 \times 10^1 T^3 + \\ 1.9701130 \times 10^3 T^2 - 1.005187 \times 10^5 T + 2.0678544 \times 10^6$$

Thermal conductivity (W/m-K)

$$K_{\ell} = 3.586226 \times 10^{-10} T^5 - 1.6795344 \times 10^{-7} T^4 + \\ 3.120013 \times 10^{-5} T^3 - 2.8859648 \times 10^{-3} T^2 + \\ 1.3152021 \times 10^{-1} T - 2.182878$$

Specific heat (J/Kg-K)

$$c_{\ell} = 3.543145 \times 10^{-4} T^4 - 1.0894305 \times 10^{-1} T^3 + \\ 1.2632769 \times 10^1 T^2 - 6.500754 \times 10^2 T + 1.4495738 \times 10^4$$

Properties of 304 stainless steel

Thermal conductivity (w/m-K)

$$K_p = - 2.25468 \times 10^{-4} T^2 + 9.99792 \times 10^{-2} T + 2.2549$$

Specific heat (J/Kg-K)

$$C_p = - 1.037895 \times 10^{-2} T^2 + 4.982373 T - 1.5772696 \times 10^2$$

Specific heat of Aluminum (J/Kg-K)

$$C_{Al} = - 8.1727423 \times 10^{-5} T^3 - 4.3008433 \times 10^{-3} T^2 + \\ 8.9683338 T - 2.8647838 \times 10^2$$

APPENDIX C

WICK-WALL INTERFACE NODES

Due to the change of variables used (see Appendix A) nodes are spaced exponentially through the wall and wick. It was found that for best results three nodes were needed in the wall and two in the wick with one for the interface. The wick nodes are smaller than the wall nodes and a scale factor SF was calculated so that the same value of DX could be used. Figure 27 shows nodes near the interface in the evaporator.

To place the fourth node on the interface of the wick and wall an artificial radius had to be calculated. This artificial radius was then used for calculating the locations of all nodes in the wall and the scale factor for the nodes in the wick.

The artificial radius is given by:

$$r_{art} = \left[\frac{r_0}{r_B} \right]^{1/(NIE-1)} \frac{(NIE-1)}{(2-NIE)}$$

Wick nodes are smaller than wall nodes by the factor SF given by:

$$SF = \frac{1}{2} (NIE-2) \ln(r_B/r_I) / \ln(r_0/r_{art})$$

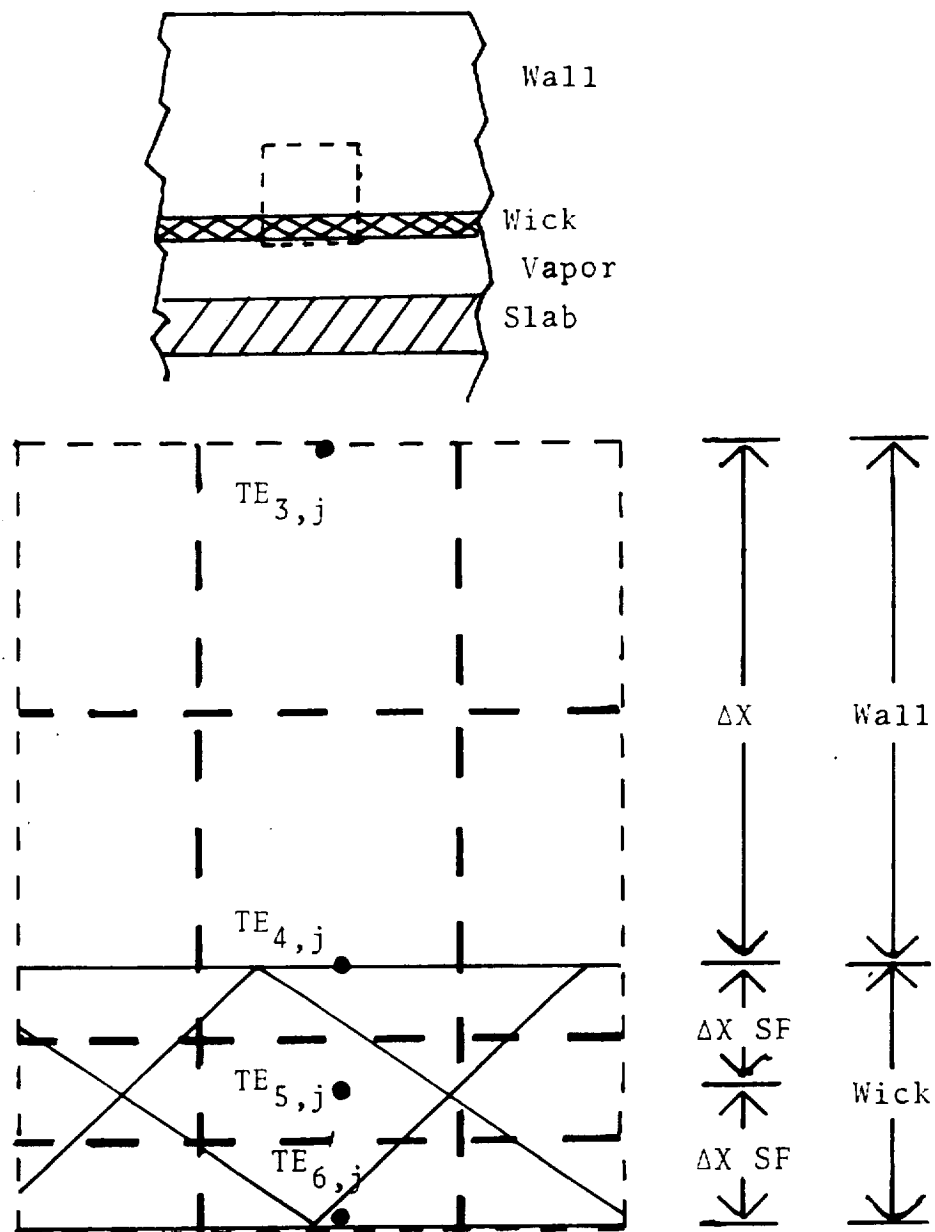


Figure 27. Wick-Wall Interface Nodes

A heat balance on node 4 gives:

$$r_4^2 \rho_4 c_4 \Delta z \Delta y \left(\frac{\Delta x + SF \Delta x}{2} \right) \frac{TE_{4,j}^{n+1/2} - TE_{4,j}^n}{t^{n+1/2} - t^n} = \frac{K_p}{\Delta x} \Delta y \Delta z (TE_{3,j}^{n+1/2} - TE_{4,j}^{n+1/2})$$

$$\frac{K_w}{\Delta x SF} \Delta y \Delta z (TE_{5,j}^{n+1/2} - TE_{4,j}^n) + \frac{K_p}{\Delta y} \Delta z \left(\frac{\Delta x + SF \Delta x}{2} \right) (TE_{4,j+1}^n + TE_{4,j-1}^n - 2TE_{4,j}^n)$$

which can be rearranged for the subroutine to give

$$\begin{aligned} & - \left(\frac{K_p \Delta t}{2(\Delta x)^2 (1+SF) \rho_4 c_4 r_4^2} \right) TE_{3,j}^{n+1/2} + \left(1 + \frac{K_p \Delta t}{2(\Delta x)^2 (1+SF) \rho_4 c_4 r_4^2} \right) \\ & \quad \left(\frac{K_w \Delta t}{2(\Delta x)^2 SF (1+SF) \rho_4 c_4 r_4^2} \right) TE_{4,j}^{n+1/2} \\ & - \left(\frac{K_w \Delta t}{2(\Delta x)^2 SF (1+SF) \rho_4 c_4 r_4^2} \right) TE_{5,j}^{n+1/2} = \frac{K_p \Delta t}{2(\Delta y)^2 \rho_4 c_4 r_4^2} (TE_{4,j+1}^n + TE_{4,j-1}^n - 2TE_{4,j}^n) + TE_{4,j}^n \end{aligned}$$

APPENDIX D

COMPUTER CODE



```

PRO, 44 MAIN (INPUT, OUTPUT, TAPE5=INPUT, TAPE6=OUTPUT
1. DATA, TAPE2=DATA, LIST, TAPE7=LIST)
DIMENSION IF (6,70), TC (6,30), T (6,30), D (30), Z (20), F (70), W (70)
1. ATE (6), ATC (6), AJ1 (6), AYE (6,30), AYC (6,30), AXC (6,30), AYC (6,30)
1. A (30), OXE (6,70), CYF (6,70), CYC (6,70), CYC (6,30), AXCON (6), PSI2 (6)
1. , OCV (15)
COMMON ET, TS, CIS, TE, TV, TC, TR, CIE, OR, DEV, OCP, QMAX, NIE, NJE, NIC, NJC
1. LWFE, LWFC, LBO, LNA, CXF, CYF, CXG, CYG, CV, V, TL, EL, ASU, BSU, XL, CC, ICRIT
1. AYE, AYC, AXG, AYC, AV, BV, AS, BS, AC, BC, CIE, CIG, AIE, AIG
1. MDOT, PMASS, DT, DT0, IX, KF, F, G, DXG, OYC, CL, NJA, CPRESIST
1. WT, OF, RF, NL, BETA, PORSTY
REAL NL, KL, MDOT, KF, HFG, KW
WRITE (6,65)
65  FORMAT ("INPUT CASE NUMBER")
READ (5,*) NO
WRITE (6,75)
75  FORMAT ("INPUT DT, NOT")
READ (5,*) DT, NOT
WRITE (6,85)
85  FORMAT ("INPUT MDOT, PMASS, DIS, DIP, AR, TI, CPRESIST")
READ (5,*) MDOT, PMASS, DIS, DIP, AR, TI, CPRESIST
WRITE (6,100)
100 FORMAT ("TYPE 1 TO INPUT ALL DATA")
READ (5,*) INPUT
IF (INPUT.NE.1) GO TO 250
WRITE (6,200)
200 FORMAT ("INPUT NIE, NJE, NIC, NJC, NJA")
READ (5,*) NIE, NJE, NIC, NJC, NJA
WRITE (6,300)
300 FORMAT ("INPUT TSI, TEI, TVI, TCI, TRI")
READ (5,*) TSI, TEI, TVI, TCI, TRI
WRITE (6,400)
400 FORMAT ("INPUT LWFE, LBO, LWFC, LNA")
READ (5,*) LWFE, LBO, LWFC, LNA
WRITE (6,450)
450 FORMAT ("INPUT WT, OF, RF, NL, BETA, PORSTY")
READ (5,*) WT, OF, RF, NL, BETA, PORSTY
C INITIALIZE VALUES
ET=0
TS=TSI
DO 2 J=1, NJE
DO 1 I=1, NIE
1  TE (I, J)=TEI
2  CONTINUE
TV=TVI
DO 4 I=1, NIC
DO 3 J=1, NJC
3  TC (I, J)=TCI
4  CONTINUE
TR=TRI
XL=.1524
GO TO 350
250 CALL DATAIN
350 DT0=DT
ET=0.
WRITE (3,500) PMASS, AR, MDOT
500 FORMAT (5X, "MASS OF HEAT SINK", F11.3, 1X, "KG AREA", F11.3, 1X,
1 "M**2", 5X, "FLOW RATE", 3X, 1P15.6, 3X, "KG/SEC")
DO 5 I=1, NIE
ATC (I)=0.
DO 5 J=1, NJE
5  ATE (I)=TE (I, J)+ATE (I)
6  ATE (I)=ATE (I)/FLOAT (NJE)

```



```

      EM=1.72
      ICOUNT=0
      OPTV=TV
      DF=1.91E-05
      PF=1.59E-05
      PORSTY=.595
      SMAIS=1.E+22
      LWFC=LWFC
      WRITE(3,402)NO
402  FORMAT(13,"CASE NUMBER" ,I4)
      CALL PAPAMTR
      GP=5.8537E-8*FV**4P*TP**4+CC*(TR-TI)
      CALL OUTPUT
C  START TIME CYCLES
      DO 100J N=1,NOI
      ICOUNT=ICOUNT+1
      IF (LWFC.EQ.LWFCO) GO TO 20
      CALL PAPAMTR
      OPTV=TV
      LWFC=LWFC
      GO TO 40
20  IF(ABS(TV-OPTV).LT..1) GO TO 30
      CALL PAPAMTR
      OPTV=TV
      GO TO 30
30  IF(ABS(OT-5).LT..001) GO TO 50
      IF(N-10)80,80,40
40  IF(ABS(TR-TPO)-.001)50,80,40
50  IF(ABS(TV-TVO)-.001)55,80,80
55  OT=2*OT
      IF(OT-30)70,70,60
60  OT=30
70  CALL PAPAMTR
      OPTV=TV
80  ET=ET+OT
      DO 90 I=1,NIE
90  AXCON(I)=(TC(I,2)-ATE(I))*KF/(DYC**2*NJE*R*C*ATE(I))
      TPO=TR
      TVO=TV
      CALL VAPOR
      CALL COOLER(AC,BC,CC,FI,TC,NJC,NJA,TR,EM,AR,GIP,OR,QCP)
      CALL GRID2D (TC,AXC,AYC,CXC,CYC,NIC,NJC,ATC,
1AIC,TV,ATC,C.,TS,1.,1.,1.,2,1,2,2,0,CIE,1.,LWFC,LBO)
      DO 11 I=1,NIE
      ATE(I)=0.0
      DO 10 J=1,NJE
10  ATE(I)=IE(I,J)*ATE(I)
11  ATE(I)=ATE(I)/FLOAT(NJE)
      CALL GRID2D (TC,AXC,AYC,CXC,CYC,NIC,NJC,ATC,
1AIC,TV,ATE,C.,TP,1.,1.,1.,3,1,1,2,NJA,CIC,CJC,LWFC,LNA)
      NJAP1=NJA+1
      IF(ICOUNT.EQ.5) GO TO 12
      GO TO 100
12  CALL OUTPUT
      ICOUNT=0
1000 CONTINUE
      CALL DATAOUT
      STOP
      END

```

```

SUBROUTINE PARAMTR
  DIMENSION TC(6,30),TC1(6,30),AXE(6,30),AYE(6,30),AXC(6,30),
  1AYC(6,30),CXE(6,30),CYE(6,30),CXC(6,30),CYC(6,30),AXCON(6)
  1,PSI(6)
  COMMON ET,TS,DIS,TE,TV,TC,TR,CIP,OP,OFV,OCR,CNAX,NIF,NUE,NIC,NJC
  1,LHFC,LWFC,LBO,CNA,CXE,CYE,CXC,CYC,CV,V,TL,EL,ASU,BSU,XL,CC,ICPIT
  1,AXI,AYI,AXC,AYC,AV,RV,AS,BS,AC,BC,CIE,CIC,AIE,AIC
  1,MOT,PHANS,DI,OTO,IX,KF,P,C,CXC,DYC,CL,NJA,CRESIST
  1,WT,OF,KF,NL,BETA,ROPSI
  REAL NL,KL,MOT,KF,HFG,KW,HCPSLAB
  CTV=TV
  IF (CTV.GT.125) CTV=125
C VISCOSITY (N SEC/M**2)
  XMU=-2.25319E-11*CTV**4+6.541176E-9*CTV**3-5.51203E-7*CTV**2
  1 +2.718194E-5*CTV+1.1352966E-3
C SURFACE TENSION (N/M)
  SIGMA=1.126412E-9*CTV**4-.7919365E-6*CTV**3+.5631364E-4*CTV**2
  1 -.343409E-2*CTV+1.1166917E-1
C INVERSE PERMEABILITY OF SLAB (1/M**2)
  FK=5.965E3
C PORE RADIUS (M)
  RPORE=1.915E-5
C DENSITY OF PIPE WALL (KG/M**3)
  P=7817
C SPECIFIC HEAT OF PIPE WALL (WATT SEC/KG K)
  C=-1.137895E-2*CTV**2+4.982373*CTV-1.5772696E2
C SPECIFIC HEAT OF SADDLE (WATT SEC/KG K)
  CS=-8.172742E-5*CTV**3-4.3018433E-3*CTV**2+8.9683338*CTV
  1 -2.8647819E2
C OUTSIDE RADIUS OF PIPE (M)
  RO=.00535
C EMISSIVITY OF HEAT SINK
  EM=.72
C HEAT PIPE TOTAL LENGTH (M)
  TL=.9144
C EVAPORATOR LENGTH (M)
  EL=.1524
C CONDENSER LENGTH (M)
  CL=.3048
C VAPOR DENSITY (KG/M**3)
  RHOV=8.40
C SPECIFIC HEAT OF VAPOR (WATT SEC/KG K)
  CV=1172.30
  PR=RO-AT
  PI=RB-4.0*RF*NL-BETA*(NL-1.0)
  PSUM=.0
  NI=INT(NL)
  DO 40 I=1,NI
  FI=FLOAT(I)
  TER1=ALOG((RO-(FI-1.0)*4.0*PF-(FI-1.0)*BETA)/(RB-4.0*FI*RF-(FI-1)
  C*BETA))
  PSUM=TER1+PSUM
40 CONTINUE
  SUM4=PSUM
  PSUM=.0
  NM1=NI-1
  DO 42 I=1,NM1
  FI=FLOAT(I)
  TER1=ALOG((RB-4.0*FI*RF-(FI-1.0)*BETA)/(RO-4.0*FI*RF-(FI-1)
  C*BETA))
  PSUM=TER1+PSUM
42 CONTINUE
  SUM1=PSUM
  IF (NM1.EQ.0) SUM1=0.0
C

```

```

C SET DXE=1E-06,XCO,YCO, AND DT
      NIEM1=NIE-1
      NIFM2=NIE-2
      NICM2=NIC-2
      NUJM1=NJE-1
      NIUM1=NIG-1
      NJUM1=NJC-1
      ROGUS=(RO**2./FLOAT(NIFM2))/ (PP)**
      1 (FLOAT(NIEM2)/(1.-FLOAT(NIEM2)))

      DXE=(ALOG(PO/-ROGUS))/FLOAT(NIEM2)
      DYE=.253/FLOAT(NJFM1)
      DYU=(ALOG(PO/-ROGUS))/FLOAT(NIUM2)
      DYC=(TL-EL)/FLOAT(NJCM1-1)

C THERMAL CONDUCTIVITY OF STAINLESS STEEL (WATT/M K)
      KE=-2.25468E-4*CTV**2.+2.99792E-2*CTV+2.2549
C THERMAL CONDUCTIVITY OF LIQUID NITROGEN (WATT/M K)
      KL=3.535226E-10*CTV**5.-1.579534E-7*CTV**4.+
      C+3.127013E-5*CTV**3.-2.452644E-3*CTV**2.+1.315202E-1*CTV
      C-2.182375
C THERMAL CONDUCTIVITY OF SCREEN (WATT/M K)
10    KW=KL/(OEF/(2.*PF))*(2.*(KL/KE)+OEF/(2.*PF)
      C-2.011)+2.*(KL/(OEF/(2.*PF)))+(KL/KE)*((2.*PF)/
      C(OEF-2.*PF)+1.0))+KL/(2.*PF/(OEF-2.*PF)+1.0)**2.0
C THERMAL CONDUCTIVITY OF WICK (WATT/M K)
      KW=(KW*SUMA+KL*SUMB)/(SUMA+SUMB)
C DENSITY OF LIQUID NITROGEN (KG/M**3)
      RHOL=-5.7744E-10*CTV**7+2.45756E-7*CTV**6-3.49017E-5*CTV**5
      1 +9.3731E-4*CTV**4+2.7794E-1*CTV**3-7.10677E1*CTV**2
      1 +1.31038E3*CTV-1.94571E4
C DENSITY OF WICK (KG/M**3)
      RHOW=(SUMA*(PORSTY*RHOL+(1.-PORSTY)*R)+SUMB*RHOL)/(SUMA+SUMB)
C SPECIFIC HEAT OF LIQUID NITROGEN (WATT SEC/KG K)
      CPL=3.57343E-4*CTV**4-1.089430E-1*CTV**3+1.2632769E1*CTV**2
      1 -6.5077540E2*CTV+1.4495734E4
C HEAT OF VAPORIZATION (WATT SEC/KG)
      HFG=-7.2519E18E-6*CTV**6+9.183185E-4*CTV**5
      1 -3.432252E-2*CTV**4-1.3974675E+1*CTV**3
      1 +1.0701130E+3*CTV**2-1.055187E+5*CTV
      1 +2.1670544E+6
2000  FORMAT(4E15.6)
C SLAB PROPERTIES
      DELA=7.437E-5
      DELB=6.214E-4
      NLA=4
      NLB=5
      EA=.576
      EP=.6532
      FPCINWL=(NJC-LWFC)/NJCM1
      MCPSLA=2.*TL*PI*(DELA*NLA*(EA*PHOL*CPL+FPCINWL+(1.-EA)*R*C)
      1 +DELB*NLB*(EB*PHOL*CPL+FPCINWL+(1.-EB)*R*C))
C SPECIFIC HEAT OF THE WICK (WATT SEC/KG K)
      CW=((1.-PORSTY)*P*C+PORSTY*RHL)/((1.-PORSTY)*P+PORSTY*RHOL)
      CW=(CW*SUMA+CPL*SUMB)/(SUMA+SUMB)
      WRITE(3,2001) C,CPL,FPCINWL,RHOL
C DIMENSIONS OF COOLING JACKET (M)
      ROC=.0157
      ROI=.1133
      EW=.00318
      RMAGS1=.141E*((DL*(ROC**2-ROI**2)+2.*EW*(ROC**2+ROI**2))*C*R
      1 *CL*(ROI**2--OC**2)*CPL*RHOL)
      IF(40)F.LT.(1.E-7) GO TO 11
      RMAGS=RMAGS1
      GSE1

```

```

11      CC=MOOT+CPL

      CIE=KF*DT/(9*C*DXE**2.*F0**2.)
      CIG=DT/CPESIST/(P*C*DXC*2.*P0)
      AC=6.243*CL*P0/(CPESIST)
      QC=DT/(PMASS*CS)
      AIE=-KX*QIS/(KF*6.2432*EL)
      AIG=-KF*CPESIST/(DXC*P0)
      AGU=2.*SIGMA/(PPURE*PHOL)
      RSU=EK*XMU/PHOL
      QMAX=4*SIGMA*PI*(NLA*DEL4+NLR*DEL6)*PHOL/
1      (PPURE*EK*XMU*(TL-(EL+CL)/2.))*HFG

      DO 200 I=1,NIE*2
      L=NIE*2-I+1
      RSI2(I)=(RPOGUS*(P0/RPOGUS)**(FLOAT(L-1)/NIE*2))**2
      DO 100 J=1,NJE
      AXE(I,J)=KF*DT/(DXE**2.*F0**2.*RSI2(I))
      AYE(I,J)=KF*DT/(DYE**2.*P0**2.*RSI2(I))
      CXE(I,J)=AXE(I,J)
      CYE(I,J)=AYE(I,J)
100    CONTINUE
200    SF=5*NIE*2*ALOG(SQRT(PRI2(NIE*2))/PI)/ALOG(P0/RPOGUS)
      PRI2=PI**2
      RNIM12=(RPOGUS*(P0/RPOGUS)**(7/NIE*2/2))**2
      PINM02=(PI*(SQRT(PRI2(NIE*2))/PI)**.75)**2
      PRI2(NIE*2)=(PI*(SQRT(PRI2(NIE*2))/PI)**.5)**2
      XDSH=((PRI2(NIE*2)-PINM02)*PHOW*CW+(RNIM12-PRI2(NIE*2))*R*C)/
2      (RNIM12-PINM02)
      AV=TKW*DT*2.*DYE*EL/(DXE*(PHOV*TL*(3.1416*RI2-
12      *PI*SLBTHK)*CV+MCPSLAB*TL*(PINM02-RI2)*
2      3.1416*CW)*SF)
      BV=TKW*DT*2.*6.243*DYC/(DXC*(PHOV*TL*(3.1416*RI2-
12      *PI*SLBTHK)*CV+MCPSLAB*TL*(PINM02-RI2)*
2      3.1416*CW)*SF)
      IX=INT(AV*NJE+BV*NJC)+10
      AV=AV/FLOAT(IX)
      BV=BV/FLOAT(IX)
      CV=TKW*DYF*EL/(DXE*SF)
      WRITE(3,2000) PMASS,CW,MCPSLAB,CS

10000  FORMAT(2F13.5)

      DO 300 J=1,NJE
      AXE(NIE*2,J)=KF*DT/(DXE**2*XDSH*(1.+SF)*PRI2(NIE*2))
      CXE(NIE*2,J)=TKW*DT/(DXE**2*XDSH*(1.+SF)*RSI2(NIE*2)*SF)
      AYE(NIE*2,J)=KF*DT/(DYE**2*XDSH*2.*RSI2(NIE*2))
      CYE(NIE*2,J)=AYE(NIE*2,J)
      CXE(NIE*1,J)=TKW*DT/(DXE**2*SF**2*CW*PHOW*2*RSI2(NIE*1))
      AXE(NIE*1,J)=CXE(NIE*1,J)
      AYE(NIE*1,J)=TKW*DT/(DYE**2*PHOW*CW*2.*PI2)
      CYE(NIE*1,J)=AYE(NIE*1,J)
      AXE(NIE,J)=PRI2(NIE*1)/RI2*CXE(NIE*1,J)
      CXE(NIE,J)=AXE(NIE,J)
      AYE(NIE,J)=TKW*DT/(DYE**2*PHOW*CW*2.*RI2)
300    CYE(NIE,J)=AYE(NIE,J)

      DO 500 I=1,NIE*2
      DO 400 J=1,NJC
      AXG(I,J)=KF*DT/(DXC**2.*P0**2.*RSI2(I))
      AYG(I,J)=KF*DT/(DYC**2.*P0**2.)
      CXG(I,J)=AXG(I,J)
400    CYG(I,J)=AYG(I,J)

```



```

500  CONTINUE
      DO 600 J=1,NJC
        AXG(NIC12,J)=KF*DT/(DYC**2*YOSH*(1.+SF)*PSI2(NICM2))
        AYG(NIC11,J)=IKY*DT/(DYC**2*PHOW*CW*2.)
        AYG(NIC12,J)=KF*DT/(DYC**2*XOSH*2.)
        CYC(NIC12,J)=AYG(NIC12,J)
        CYC(NIC11,J)=AYG(NIC11,J)
        CXG(NIC12,J)=IKW*DT/(DXC**2*YOSH*(1.+SF)*PSI2(NICM2)*SF)
        DXG(NIC11,J)=IKY*DT/(DXC**2*SF**2*CH*PHOW*2*PSI2(NICM1))
        AXG(NIC11,J)=CXG(NIC11,J)
        CYC(NIC,J)=IKW*DT/(DYC**2*PHOW*CW*2.)
        AYG(NIC,J)=CYC(NIC,J)
        AXG(NIC,J)=PSI2(NICM1)/PI2*CYC(NIC11,J)
600  CXG(NIC,J)=AXG(NIC,J)
      RETURN
    END

```

```

SUMTIME=VAPOR
DIA=1.0,IPH=1.0,TO(6,70),AXE(6,30),AYE(6,30),AXD(6,30),
1AYD(6,30),CXE(6,30),CYE(6,30),CXD(6,30),CYD(6,30),AXCON(6)
1,DDV(15)
COMMON FT,TS,DIG,TE,TU,TC,TF,DIF,QR,Q-V,CCR,CMAX,NIF,NJE,NIC,NJC
1,LWFC,LWFC,LRO,LNA,CXE,CYE,CXC,CYC,CV,V,TL,FL,ASU,RSU,XL,CC,ICRIT
1,AXE,AYE,AXD,AYD,AV,DV,AS,BS,AC,BC,CIC,CIC,AIE,AIC
1,MDOCT,PHASS,DT,DT,IX,KF,P,C,DXC,DYC,LL,NJA,CRESIST
1,WT,UF,PF,HL,BETA,PORSTY
REAL ML,KL,MDOCT,KF,HFG,KW
GO TO 200
XLRO=NJE*(1/(1+ABS(DEV)/CMAX))+1
XLNA=(NIC-NJA)*DEV/CMAX+NJA+1
LRO=INT(XLRO)+INT(2*(XLRO-INT(XLRO)))
TF(LRO,GT,(NJE+1)) LPO=NJE+1
LNA=INT(XLNA)+INT(2*(XLNA-INT(XLNA)))
IF(LNA.LE,(NJA+1)) GO TO 100
IF(LNA.GT,(NJC+1)) GO TO 70
GO TO 200
39 LNA=NJC+1
GO TO 200
100 LNA=NJA+2
200 NJAP1=NJA+1
SUMTC=0.0
DO 28 J=NJAP1,NJC
24 SUMTC=SUMTC+TO(NICM1,J)
SUMTC=SUMTC/FLOAT(NJC-NJA)
IF(SUMTC.GT.125) GO TO 50
IF(ICRIT.LT.1) GO TO 55
DO 29 I=1,1000
V=DT/1000*(ASU-RSU*V*XL-V**2)/XL+V
XL=XL+V*DT/1000
29 CONTINUE
IF(XL.GT.(TL-CL/2.)) ICRIT=0
LOF=INT(FLOAT(NJC-NJA)/2)+INT(XL/DYC)+INT(2*(XL/DYC-INT(XL/DYC)))
1 +1
LWFC=NJC-LOF
IF(LWFC-NJA) 39,30,30
30 LWFC=NJA
GO TO 45
35 IF(LWFC-1) 40,45,45
40 LWFC=1
XLRO=(XL-TL+CL/2+EL)/CL*NJE
LRO=INT(XLRO)+INT(2*(XLRO-INT(XLRO)))+1
IF(LRO.GT.(NJE+1)) LRO=NJE+1
45 GO TO 55
50 LWFC=NJC
LRO=1
ICRIT=1
55 CONTINUE
IF(LLO.EQ.1) GO TO 1001
DEV=0.
OCV(1)=.5*CV
OCV(NJE)=.5*CV
NJE41=NJE-1
DO 44 J=2,NJE41
994 OCV(J)=CV
ICRIT=0
DO 100 J=1,NJE
IF (IR0.EQ.1) GO TO 1000
DEV=OCV(J)*(T-NIE-1,J)-IF(NIE,J)+DEV
IF (DEV.LT.CMAX) GO TO 1000
IT0=1

```

```

      ICRIT=1
      LPO=J+1
1000  CONTINUE
1001  CONTINUE
      AVET=0.0
      AVETV=0.
      AVETCV=0.
      AVETC=0.0
      LROM1=LRO-1
      LNAM1=LNAM-1
      LWFCP1=LWFC+1
      LWFCP1=LWFC+1
      EACTIVE=FLOAT(LROM1-LWFCP1+1)
      CACTIVE=FLOAT(LNAM1-LWFCP1+1)
      IF (LPO.LE.LWFCP1) GO TO 14
      DO 10 J=LWFCP1,LROM1
10     AVETE=AVETE+TE(NIF,J)
10     AVETE=AVETE+TE(NIF-1,J)
10     AVETV=AVETE/CACTIVE
10     AVETC=AVETE/CACTIVE
10     IF (NIF-LROM1) 11,11,12
11     CACTIVE=CACTIVE-.5
12     IF (2-LWFCP1) 16,13,13
13     CACTIVE=CACTIVE-.5
13     GO TO 15
14     EACTIVE=0.0
15     IF (LNA.LE.LWFCP1) GO TO 24
16     DO 20 J=LWFCP1,LNAM1
20     AVETCV=AVETCV+TC(NIC,J)
20     AVETC=AVETC+TC(NIC-1,J)
20     AVETCV=AVETCV/CACTIVE
20     AVETC=AVETC/CACTIVE
20     IF (NIC-LNAM1) 21,21,22
21     CACTIVE=CACTIVE-.5
22     IF (2-LWFCP1) 25,23,23
23     CACTIVE=CACTIVE-.5
23     GO TO 25
24     CACTIVE=0.0
25     TVO=TV
25     DO 26 I=1,IX
26     TV=AV*CACTIVE*(AVETE-AVETV-TV+TVO)+TV
26     TV=AV*CACTIVE*(AVETC-TVO-TV+TVO)
26     TV=(TV-TVO)*OT/OTQ+TVO
26     OTQ=OT
      WRITE(3,4) LPO, LNA, LWFC, V, XL
49  FORMAT('I4,2E16.5')
897  FORMAT('E15.8')
      RETURN
      END

```

```

SUBROUTINE COOLIP (A,C,D,II,I,NJC,NJA,TR,E,AF,QIR,QP,QCR)
  DIMENSION T(6,30)
  SUMT=0.0
  QP=H.66)7E-H+E*AP+TS**4+C*(TR-TI)
  NJAP1=NJA+1
  DO 10 J=NJAP1,NJC
    SUMT=SUMT+T(1,J)-TR
  10 QP=H*SUMT/FLCAT(NJC-NJA)
    TR=3*(QCR+QIR-QP)+TR
  RETURN
END

```



```

      SUBROUTINE SPID2D (I,AX,AY,CY,CY,NI,NJ,AXIAL,AI1,AIM,AJ1,AJM,
      1QI1,QIM,QMI,QJM,LI1,LIM,LJ1,LJM,NJA,QI1,QJ1,LWF,LRO)
      DIMENSION T(6,30),D(30),W(70),E(70),F(30),AJ1(6),AX(6,70),
      1AY(6,30),CX(6,30),CY(6,30),A(70),C(30),AXIAL(6)

      NIM=NI-1
      NJM=NJ-1
      C MAKE I SWEEP
      C PICK LEFT BOUNDARY CONDITION
      12 IF (LJ1-2) 14,16,100
      14 DO 15 I=2,NIM
      15 Q(I)=AJ1(I)
      GO TO 100
      16 DO 17 I=2,NIM
      17 Q(I)=(1.-2.*AY(I,1))*T(I,1)+2.*AY(I,1)*T(I,2)+T(I,1)*AXIAL(I)
      GO TO 100
      100 IF(1-NJA)200,200,300
      200 LIN=2
      AIM=0.0
      GO TO 400
      300 LIN=LI1
      AIM=AI1
      400 CONTINUE
      IF(1-LWF)600,600,500
      500 IF(1-LRO)700,600,600
      600 LIO=2
      AIO=0.0
      GO TO 800
      700 LIO=LIM
      AIO=AIM
      800 CONTINUE
      DO 1000 I=1,NI
      A(I)=AX(I,1)
      C(I)=CX(I,1)
      1000 CALL PDACHE (A,C,D,NI,E,F,W,LIN,LIO,
      1AIM,AIO,QI1,QIM)
      21 DO 40 J=2,NJM
      DO 25 I=2,NIM
      25 Q(I)=CY(I,J)*T(I,J+1)+AY(I,J)*T(I,J-1)
      1+(1.-AY(I,J)-CY(I,J))*T(I,J)+T(I,J)*AXIAL(I)
      DO 30 I=1,NI
      30 T(I,J-1)=Q(I)
      101 IF(J-NJA)201,201,301
      201 LIN=2
      AIM=0.0
      GO TO 401
      301 LIN=LI1
      AIM=AI1
      401 CONTINUE
      IF(J-LWF)601,601,501
      501 IF(J-LRO)701,601,601
      601 LIO=2
      AIO=0.0
      GO TO 801
      701 LIO=LIM
      AIO=AIM
      801 CONTINUE
      DO 1001 I=1,NI
      A(I)=AX(I,J)
      C(I)=CX(I,J)
      1001 CALL PDACHE (A,C,D,NI,E,F,W,LIN,LIO,
      1AIM,AIO,QI1,QIM)
      40 CONTINUE

```

```

C PICK RIGHT BOUNDARY CONDITION
DO 44 I=2,NIM
44 D(I)=(1.-2.*AX(I,NJ))*T(I,NJ)+2.*AX(I,NJ)*T(I,NJ-1)
1 + T(I,NJ)*AXIAL(I)
47 DO 50 I=1,NI
37 T(I,NJ-1)=W(I)
IF(NJ-LNF)602,602,502
502 IF(NJ-L10)712,602,602
602 LID=2
AID=0.0
GO TO 402
702 LID=LIM
AID=AI1
802 CONTINUE
DO 1002 I=1,NI
A(I)=AX(I,NJ)
1002 C(I)=CX(I,NJ)
CALL ROACHE (A,C,D,NI,E,F,W,L11,L10,
1AI1,AID,0I1,0IM)
DO 48 I=1,NI
48 T(I,NJ)=W(I)
C MAKE J SWEEP
IF (L11-2) 53,51,53
49 DO 52 J=1,NJ
50 D(J)=AI1
GO TO 55
51 DO 52 J=2,NJM1
52 D(J)=(1.-2.*AX(1,J))*T(1,J)+2.*AX(1,J)*T(2,J)-CI1*AI1
GO TO 55
53 DO 54 J=2,NJM1
102 IF(J-NJ)202,202,302
202 LIN=2
CIN=0.0
GO TO 402
302 LIN=L11
CIN=CI1
402 CONTINUE
D(J)=(1.-2.*AX(1,J)-2.*CIN)*T(1,J)+2.*AX(1,J)*T(2,J)
1+(2.*CIN)*0I1+T(1,J)*AXIAL(1)
54 IF(LIN.EQ.1) D(J)=AI1
DO 1003 J=1,NJ
A(J)=AY(1,J)
1003 C(J)=CY(1,J)
55 CALL ROACHE (A,C,D,NJ,E,F,W,LJ1,LJM,
1AJ1(1),AJM,0J1,0JM)
DO 70 I=2,NIM1
DO 60 J=2,NJM1
60 D(IJ)=CX(I,J)*T(I+1,J)+AX(I,J)*T(I-1,J)
1+(1.-AX(I,J)-CX(I,J))*T(I,J)+T(I,J)*AXIAL(I)
DO 65 I=1,NJ
65 T(I-1,J)=A(J)
DO 1004 J=1,NJ
A(J)=AY(I,J)
1004 C(J)=CY(I,J)
CALL ROACHE (A,C,D,NJ,E,F,W,LJ1,LJM,
1AJ1(I),AJM,CJ1,0JM)
70 CONTINUE
C PICK BOTTOM BOUNDARY CONDITION
DO 75 J=1,NJ
IF(J-L40)73,73,72
72 IF(J-L30)74,73,73
73 D(IJ)=(1.-2.*CX(NI,J))*T(NI,J)+2*AX(NI,J)*T(NI-1,J)
1 + T(NI,J)*AXIAL(NI)
GO TO 75

```

```
74   D(J)=A(I)
75   CONTINUE
      DO 69 J=1,NJ
69   T(NI-1,J)=W(J)
      DO 1005 J=1,NJ
      A(J)=AY(NI,J)
1005  C(J)=CY(NI,J)
      CALL POACHE (A,C,D,NJ,E,F,W,LJ1,LJM,
1AJ1(NI),AJM,QJ1,QJM)
      DO 74 J=1,NJ
74   T(NI,J)=W(J)
      RETURN
      END
```

```

SUBROUTINE ROACHF (A,C,M,MD,F,F,W,L1,LM,A1,AM,
1Q1,QM)
DIMENSION A(MD),C(MD),Q(MD),F(4D),F(MD),W(MD)
IF (L1-2) 1,2,3
1  E(1)=0
  F(1)=A1
  GO TO 8
2  E(1)=1.
  F(1)=-A1
  GO TO 4
3  E(1)=A1/(A1-1.)
  F(1)=Q1/(1.-A1)
4  MM=MD-1
  DO 5  I=2,MM
    DEN=1.+A(M)+C(M)-A(M)*E(M-1)
    E(M)=C(M)/DEN
5  F(M)=(Q(M)+A(M)*F(M-1))/DEN
  IF (LM-2) 6,7,8
6  W(M)=A1
  GO TO 9
7  W(M)=(F(MM)+AM)/(1.-E(MM))
  GO TO 9
8  W(M)=(F(MM)+QM/AM)/((1.+A1)/AM-E(MM))
9  DO 10  K=1,MM
    M=MD-K
10  A(M)=F(M)+W(M+1)+F(M)
  RETURN
END

```

```

SUBROUTINE OUTPUT
  DIMENSION TE(6,20),TC(6,30),AYE(6,30),AYF(6,30),AXC(6,30)
  1,AYC(6,30),CXF(6,30),CYF(6,30),AXCON(6)
  COMMON ET,TC,CTC,TE,TV,TC,TP,QIR,QF,QEV,QCP,QMAX,NIE,NJE,NIC,NJC
  1,LHFE,LHFC,LBO,LNA,CYE,CYF,CXC,CYC,CV,V,TL,EL,ASU,BSU,XL,CC,ICRIT
  1,AXC,AYE,AXC,AYC,AV,AV,AS,BS,AC,BC,CIE,CTC,AIE,AIC
  1,MOT,RMASS,DT,DTO,IX,KF,P,Q,QXC,QYC,CL,NJA,CRESIST
  1,WT,DF,CF,NL,BETA,POPSY
  REAL NL,KL,MOT,KF,HFC,KW
  WRITE(3,5)
  WRITE(3,10) ET
  WRITE(3,30)
  DO 1 I=1,NIE
  1 WRITE(3,40) (TE(I,J),J=1,NJE)
  WRITE(3,50) TV,QEV,QMAX
  WRITE(3,60)
  DO 2 I=1,NIC
  N=NIC-I+1
  2 WRITE(3,70) (TC(N,J),J=1,NJC)
  WRITE(3,80) TP,QCP,QF
  5 FORMAT(1)
  10 FORMAT(1X,"ELAPSED TIME",F8.3,1X,"SECONDS")
  30 FORMAT(5X,"EVAPORATOR GRID")
  40 FORMAT(5CF8.3)
  50 FORMAT(5X,"VAPOR TEMPERATURE",F8.3,3X,"HEAT IN",F8.3,3X,
  1 "QMAX",F8.3,3X,"WATTS")

  60 FORMAT(5X,"CONDENSER GRID")
  70 FORMAT(7CF8.3)
  80 FORMAT(5X,"HEAT SINK TEMPERATURE",F8.3,1X,"HEAT IN",F8.3,
  11X,"HEAT OUT",F8.3,1X,"WATTS")
  RETURN
END

```

```

SUBROUTINE DATAIN
  DIMENSION IT(6,70),TC(6,70),T(6,70),D(30),E(30),F(30),W(30)
  1,ATC(6),ATD(6),AJ1(6),AYE(6,70),AYE(6,70),AXC(6,30),AYC(6,30)
  1,A(30),CXF(6,30),CYE(6,30),CYC(6,70),CYC(6,30),AXCON(6),RSI2(6)
  COMMON IT,TS,GIC,TE,TV,TC,TP,GIF,OP,OFV,OCR,GMAX,NIE,NJE,NIC,NJC
  1,LWFE,LWFG,LRO,LNA,CXF,CYE,CXC,CYC,CV,V,TL,EL,ASU,BSU,XL,CC,ICRIT
  1,AXF,AYF,AXC,AYC,AV,RV,AS,RS,AC,RC,CIF,GIC,AIF,AIC
  1,MDO1,RMATS,DT,INFO,IX,KF,R,G,DXC,DYC,CL,NJA,CRESIST
  1,WT,OF,PF,NL,BETA,POPSY
  REAL NL,KL,MDO1,KF,HFG,KW
  READ(2,30)NIE,NJE,NIC,NJC,NJA
  READ(2,75)LWFE,LRO,LWFG,LNA,ICRIT
  READ(2,40)WT,OF,PF,NL,BETA,POPSY
  READ(2,100)TS,OSE
  DO 10 I=1,NIE
10  READ(2,200) (TE(I,J),J=1,NJE)
    READ(2,300) TV,V,XL
    DO 20 I=1,NIC
20  READ (2,400) (TC(I,J),J=1,NJC)
    READ(2,500) TP,OCR,OR
50  FORMAT(5I4)
75  FORMAT(5I4)
80  FORMAT(3E10.5,F6.2,2E10.5)
100 FORMAT(2F8.3)
200 FORMAT(10F3.7)
300 FORMAT(F8.3,2F16.5)
400 FORMAT(16F3.7)
500 FORMAT(2F8.3)
  RETURN
END

```

```

SUBROUTINE DATADAT
  DIMENSION IT(6,30),TC(6,30),T(6,30),O(3,1),F(3,1),F(3,1),W(30)
  1,AT(6,1),ATC(6),AJ1(6),AXE(6,75),AYE(6,70),AXC(6,30),AYC(6,30)
  1,AX(6),CYL(6,30),CYC(6,30),CYC(6,30),CYC(6,30),AXCON(6),KSI2(6)
  COMMON /1,TS,BIS,TE,TV,TC,TR,OR,ORV,OCR,GMAY,NIE,NJE,NIC,NJC
  1,LWFE,LWFC,LPO,LNA,CXF,CYE,CXC,CYC,CV,V,TL,EL,ASU,BSU,XL,CG,ICRIT
  1,AXF,AYF,AXC,AYC,AV,BV,AS,BS,AC,BC,CIE,CIC,AIF,AIC
  1,MDOI,K4455,DI,DFO,IX,KF,R,C,DXC,DYC,CL,NJA,CRESIST
  1,WI,OF,PF,NL,BETA,PORSTY
  REAL KL,KL,MDOI,KF,HFG,KW
  WRITE(2,50)NIE,NJE,NIC,NJC,NJA
  WRITE(2,75)LWFE,LPO,LWFC,LNA,ICRIT
  WRITE(2,80)WI,OF,PF,NL,BETA,PORSTY
  WRITE(2,100)TS,DSF
  DO 10 I=1,NIE
10  WRITE(2,200) (TE(I,J),J=1,NJF)
     WRITE(2,300) TV,V,XL
     DO 20 I=1,NIC
20  WRITE(2,400) (TC(I,J),J=1,NJC)
     WRITE(2,500) TR,OCR,OR
50  FORMAT(5I4)
75  FORMAT(5I8)
80  FORMAT(3E10.5,F6.2,2F10.5)
100 FORMAT(2F8.3)
200 FORMAT(15F8.7)
300 FORMAT(5F8.7,2F16.5)
400 FORMAT(15F8.7)
500 FORMAT(4F8.3)
  RETURN
END

```

APPENDIX E

DISCUSSION OF STABILITY AND ACCURACY
OF NUMERICAL TECHNIQUES

The technique used for solution of the vapor temperature is essentially a one dimensional heat balance of the form:

$$T_i^{n+1} = A_i T_{i+1}^n + B_i T_{i-1}^n + (1-A_i+B_i) T_i^n$$

For stability it is necessary that [16,17,18]

$$(A_i + B_i) \leq 1$$

All elements of A and B are fixed except the time step. Thus the time step must be adjusted to maintain stability.

In solving for the vapor temperature the coefficients A and B are calculated. New values are then defined by

$$A_i' = \frac{A_i}{(A_i+B_i)}$$

$$B_i' = \frac{B_i}{(A_i+B_i)}$$

The solution is then iterated $(A + B)$ times to complete one time step.

The alternating direction implicit method used in this study has an accuracy of $O(\Delta t^2, \Delta x^2, \Delta y^2)$ [16].

According to a von Neumann stability analysis the method is unconditionally stable [16,18]. However in practice this method, although it does permit larger time steps than standard explicit method, will become unstable if time steps used are too large.

APPENDIX F

CALCULATION OF THERMAL CONDUCTIVITY FOR THE WICK

Since the wick is a composite of screen and fluid gaps, a method must be developed for estimating its thermal conductivity.

The thermal conductivity of the fluid gaps is given by the polynomial expression given in Appendix B.

The thermal conductivity of the screen was calculated using the method of Williams [24].

$$\begin{aligned}
 K_s = K_\ell & \frac{1}{\frac{d_f}{2r_f} \left[2 \frac{K_\ell}{K_p} + \frac{d_f}{2r_f} - 2 \right]} \\
 & + \frac{2}{\frac{d_f}{2r_f} \left(\frac{K_\ell}{K_p} \right) \left[\frac{2r_f}{d_f - 2r_f} + 1 \right]} \\
 & + \frac{1}{\left[\frac{2r_f}{d_f - 2r_f} + 1 \right]^2}
 \end{aligned}$$

The overall thermal conductivity is then a weighted average of the values for the screen and fluid. Weighting factors are given by

$$\% \text{ screen} = \sum_{N=1}^{NL} \ln[(r_B - (4r_f + \beta)(N-1)) / (r_B - 4Nr_f - (N-1)\beta)]$$

$$\% \text{ fluid} = \sum_{N=1}^{NL-1} \ln [(r_B - 4Nr_f - (N-1)\beta) / (r_B - (4r_f + \beta)N)]$$

Total thermal conductivity is calculated to be

$$K_w = K_s (\% \text{ screen}) + K_\ell (\% \text{ fluid})$$

APPENDIX G

ANALOG SCALING

Due to the nature of the analog computer equations must be scaled before they can be solved. This scaling is accomplished by making a change of variable. Each variable in the unscaled equation is non-dimensionalized by some maximum value. For example the unscaled form of equation 4.1 is:

$$\frac{dT_1}{dt} = \frac{4\pi l_E K_p}{\rho_p c_p v_{pE} \ln(r_0/r_B)} (T_2 - T_1) + \frac{2Q_E}{\rho_p c_p v_{pE}}$$

Make the following changes of variable:

$$T^* = \frac{T - T_{\min}}{T_{\max} - T_{\min}}$$

$$Q_E^* = \frac{Q_E}{Q_{\max}}$$

$$t^* = \frac{t}{t_{\max}}$$

gives

$$\frac{(T_{\max} - T_{\min})}{t_{\max}} \frac{dT_1^*}{dt^*} = \frac{4\pi \ell_E K_p (T_{\max} - T_{\min})}{\rho_p c_{pE} \ln(r_0/r_B)} (T_2^* - T_1^*)$$

$$+ \frac{2Q_E^* Q_{\max}}{\rho_p c_{pE}}$$

which can be simplified to:

$$\frac{dT_1^*}{dt^*} = \frac{4\pi \ell_E K_p t_{\max}}{\rho_p c_{pE} \ln(r_0/r_B)} (T_2^* - T_1^*)$$

$$+ \frac{2 Q_{\max} t_{\max}}{\rho_p c_{pE} (T_{\max} - T_{\min})} Q_E^*$$

Similar scaling for each equation gives a new system of equations that differs from the first in only the time scaling term.

APPENDIX H

DERIVATION OF EXPONENTIAL MODEL

Assume entire system approximated as lumped mass with composite specific heat. Then

$$m_T c_T \frac{dT}{dt} = Q_{IN} + \dot{m}_f c_f (T_I - T)$$

Define $T^* = (T - T_I)$. Equation becomes

$$m_T c_T \frac{dT^*}{dt} = Q_{IN} - \dot{m}_f c_f T^*$$

This first order differential equation can be solved to give

$$T^* = \frac{Q_{IN}}{\dot{m}_f c_f} \left(1 - e^{-\frac{\dot{m}_f c_f}{m_T c_T} t} \right)$$

and

$$Q_{OUT} = \dot{m}_f c_f T^*$$

REFERENCES

1. Cotter, T. P., "Theory of Heat Pipes," Los Alamos Scientific Laboratory, Report LA-3246-MS, 1965.
2. Chisholm, D., The Heat Pipe, Mills and Boon Limited, London, 1971.
3. Cotter, T. P., "Heat Pipe Start-up Dynamics," presented 1967, Thermionic Conversion Specialist Conference, October 30, 1967, Palo Alto, California.
4. Williams, C. L., and G. T. Colwell, "Heat Pipe Model Accounting for Variable Evaporator and Condenser Lengths," AIAA Journal, Vol. 12, no. 9, pp. 1261-1267, September, 1974.
5. Chato, J. C., and J. H. Streckert, "Performance of a Wick-Limited Heat Pipe," ASME Publication 69-HT-20, 1969.
6. Kirkpatrick, J. P., and P. J. Brennan, "The Advanced Thermal Control Flight Experiment," presented at the AIAA 8th Thermophysics Conference, Palm Springs, California, July 16-18, 1973.
7. Sherman, A., and P. Brennan, "Cryogenic and Low Temperature Heat Pipe/Cooler Studies for Spacecraft Application," presented at the AIAA-ASME 1974 Thermophysics and Heat Transfer Conference, Boston, Massachusetts, July 15-17, 1974.
8. Hare, J. D., Performance of a Nitrogen Heat Pipe with Various Capillary Structures, M. S. Thesis, Georgia Institute of Technology, 1975.
9. Colwell, G. T., "Prediction of Cryogenic Heat Pipe Performance," Report no. 2, NASA contract NSG-2054, February, 1976.
10. Groll, M., Bost, H. Kreeb, Schubert, F. Zimmermann, "Heat Transfer Limits, Lifetests, and Dynamic Behavior of Heat Pipes," Institut fur Kernenergetik, Universitat Stuttgart, Germany.

11. Smirnov, F., V. V. Barsookov, and L. N. Mishchenko, "Engineering Methods of Low-Temperature Heat Pipe Designing Calculations," presented at the 2nd International Heat Pipe Conference, Bologna, Italy, March 21-April 2, 1976.
12. Rice, G., and E. Azad, "Dynamic Characteristics of Heat Pipes," presented at the 2nd International Heat Pipe Conference, Bologna, Italy, March 31-April 2, 1976.
13. Anand, D. K., A. Z. Dybbs, and R. E. Jenkins, "Effect of Condenser Parameters on Heat Pipe Optimization," Journal of Spacecraft, Vol. 4, No. 5, pp. 695-696, May, 1967.
14. Calimbas, and Hulett, "An Avionic Heat Pipe," ASME publication 69-HT-16, 1969.
15. Cosgrove, J. H., A. Ferrel, and A. Carnesale, "Operating Characteristics of Capillary-Limited Heat Pipes," Journal of Nuclear Energy, 1967, Vol. 21, pp. 547-558.
16. Roache, Patrick J., Computational Fluid Dynamics, Hermosa Publishers, Albuquerque, N. M., 1972.
17. Clausing, A. M., "Numerical Methods in Heat Transfer," Advanced Heat Transfer, Ed. by B. T. Chao, University of Illinois Press, Chicago, 1969.
18. Carnahan, B., H. A. Luther, and J. O. Wilkes, Applied Numerical Methods, Wiley, New York, 1957.
19. Eckert, E. R. G., and R. M. Drake, Jr., Analysis of Heat and Mass Transfer, McGraw-Hill, New York, 1972.
20. Kreith, F., Principles of Heat Transfer, Second Edition, International Textbook Co., Scranton, PA, 1966.
21. Larkin, B. K., "Some Stable Explicit Approximations to the Diffusion Equation," Mathematics of Computation, 18, 196-202, 1964.
22. Schwartz, Anthony M., "Capillarity, Theory and Practice," Industrial and Engineering Chemistry, Vol. 61, No. 1, pp. 10-21, January, 1969.
23. Scott, Russel B., Cryogenic Engineering, D. Van Nostrand Co., Inc., Princeton, N.J., 1959.

24. Williams, C. L., Correlation of Heat Pipe Parameters, Ph.D. Dissertation, Georgia Institute of Technology, 1973.
25. National Bureau of Standards, Tech. Note 648, pp. 31-32, December, 1973.
26. Saaski, E. W., "Heat Pipe Temperature Control Utilizing a Soluble Gas Absorption Reservoir," NASA CR-137, 792, February, 1976.
27. Symons, E. P., "Wicking of Liquids in Screens," NASA TN-D 7657, May, 1974.
28. Priester, D. E., "Transient Response of A Cryogenic Heat Pipe", M.S. Thesis, Georgia Institute of Technology, 1976.

